# Analysis of charge and orbital order in $Fe_3O_4$ by Fe $L_{2,3}$ resonant x-ray diffraction

A. Tanaka,[1] C. F. Chang,[2,3] M. Buchholz,[2] C. Trabant,[2,4] E. Schierle,[4] J. Schlappa,[2,4] D. Schmitz,[4] H. Ott,[2] P. Metcalf,[5] L. H. Tjeng,[2,3] and C. Schüßler-Langeheine[2,4]

[1]*Department of Quantum Matters, ADSM, Hiroshima University, Higashi-hiroshima 739-8530, Japan*
[2]*II. Physikalisches Institut, Universität zu Köln, Zülpicher Straße 77, 50937 Köln, Germany*
[3]*Max Planck Institute CPfS, Nöthnizer Straße 40, 01187 Dresden, Germany*
[4]*Helmholtz-Zentrum Berlin für Materialien und Energie GmbH, Albert-Einstein-Straße 15, 12489 Berlin, Germany*
[5]*Department of Chemistry, Purdue University, West Lafayette, Indiana 47907, USA*

(Received 16 August 2012; published 6 November 2013)

To elucidate charge and orbital order below the Verwey transition temperature $T_V \sim 125$ K, a thin layer of magnetite partially detwined by growth on the stepped MgO(001) substrate has been studied by means of soft x-ray diffraction at the Fe $L_{2,3}$ resonance. The azimuth angle, incident photon polarization, and energy dependence of the $(00\frac{1}{2})_c$ and $(001)_c$ reflection intensities have been measured, and analyzed using a configuration-interaction $FeO_6$ cluster model. The azimuth dependence of the $(00\frac{1}{2})_c$ reflection intensities directly represents the space-group symmetry of the orbital order in the initial state rather than indirectly through the intermediate-state level shifts caused by the order-induced lattice distortions. From the analysis of the $(00\frac{1}{2})_c$ reflection intensities, the orbital order in the $t_{2g}$ orbitals of $B$ sites below $T_V$ is proved to have a large monoclinic deformation with the value of $\mathrm{Re}[F_{xy}]/\mathrm{Re}[F_{yz}] \sim 2$. This finding contradicts the majority of theories on the Verwey transition so far proposed. We show that the experimentally observed resonance spectra cannot be explained by orbital and charge orders obtained with recent LDA + $U$ and GGA + $U$ band structure calculations but by a complex-number orbital order with excellent agreement.

DOI: 10.1103/PhysRevB.88.195110 PACS number(s): 75.25.Dk, 61.05.C−, 61.50.−f, 71.30.+h

## I. INTRODUCTION

Magnetite ($Fe_3O_4$) is a magnetic mineral so abundant that it was even known as a loadstone in the Greek era. Nowadays, in addition to its magnetic properties, considerable attention is drawn to a mysterious transition accompanied by a lattice deformation at temperature $T_V \sim 125$ K, where an abrupt increase of resistivity by two orders of magnitude upon cooling was discovered by Verwey in 1939.[1] Although extensive studies have been made both on experimental and theoretical sides, even after more than 70 years, the mechanism of this Verwey transition still remains a highly controversial problem.[2]

Magnetite has the inverse spinel structure with the cubic $Fd\bar{3}m$ symmetry at room temperature. One-third of Fe ions are on $A$ sites in tetrahedral oxygen coordination having a $Fe^{3+}$ formal valence, and the remaining two-thirds of Fe ions are on $B$ sites in octahedral oxygen coordination having a mixed valence state with a ratio of $Fe^{2+} : Fe^{3+} = 1 : 1$. It exhibits ferrimagnetism below $T_N \sim 860$ K, where the coupling of the magnetic moments between the $A$ and $B$ sites is antiparallel, and the net magnetization amounts to $\sim 4\,\mu_B$ per formula unit. The tetrahedral (octahedral) crystal field at the $A$ ($B$) site splits the $3d$ level into threefold $t_{2g}$ and twofold $e_g$ levels. While five electrons on each $A$ site fill up the minority-spin $3d$ orbitals on the site and essentially do not contribute to transport, the $B$ sites accommodate mobile minority-spin electrons (0.5 per site) in their $t_{2g}$ orbitals in addition to the fully occupied majority-spin $3d$ orbitals.

The crystal structure of $Fe_3O_4$ below $T_V$ is still a matter of debate. The lattice symmetry of the low-temperature phase is thought to be monoclinic[3,4] $Cc$ or triclinic[5–7] $P1$ with a $\sqrt{2}a_c \times \sqrt{2}a_c \times 2a_c$ supercell, where $a_c$ denotes the cubic lattice parameter. Iizumi *et al.* have proposed an $a_c/\sqrt{2} \times a_c/\sqrt{2} \times 2a_c$ subcell with the $P2/c$ symmetry under pseudo-orthorhombic symmetry constraints ($Pmca$ and $Pmc2_1$) on the atomic positions as approximated structure models for the low-temperature phase.[8] Recently, assuming the same structure model with the pseudo-$Pmca$ symmetry, Wright *et al.* have refined the crystal structure using x-ray and neutron powder diffraction data.[9,10] $B$ sites with two different valences +2.4 and +2.6 are found from the valence bond sum of Fe-O distances, and Jahn-Teller-like distortions of the surrounding oxygen octahedrons are observed on some of the $Fe^{2.4+}$ sites in this structure. It is only very recently that detailed atomic positions in the $C2/c$ and $Cc$ symmetries are reported.[11–13]

Verwey and co-workers have proposed a charge ordering due to electrostatic repulsion between Fe ions as the cause of the Verwey transition.[14] However, the charge ordering pattern predicted by this theory has been found to be incompatible with experimental results.[15,16] Even now, not only the ordering pattern but also the degree of charge disproportion below $T_V$ are still unsettled problems.[11,15–23]

In addition to charge ordering,[24,25] the possibilities of orbital ordering[15,26] have been discussed. Seo *et al.* have proposed a bond dimerization caused by a Peierls instability.[27] However, no evidence of dimerization below $T_V$ has been found.[10] Recently, an orbital and charge order has been predicted by band structure theory with local density approximation with Hubbard $U$ (LDA + $U$) methods[28–30] using the pseudo-$Pmca$ lattice structure data by Wright *et al.*[10] In this state, as shown in Fig. 1(a), three sites $B2a$, $B2b$, and $B3$ out of six unique $B$ sites labeled $B1a$, $B1b$, $B2a$, $B2b$, $B3$, and $B4$ in the monoclinic cell are occupied by $Fe^{3+}$ ions; each of the other three sites $B1a$, $B1b$, and $B4$ with $Fe^{2+}$ ions accommodates an extra minority-spin electron mainly in either $YZ$ or $ZX$ ($B1a,b$ sites) or $XY$ ($B4$ sites) orbital (in

 

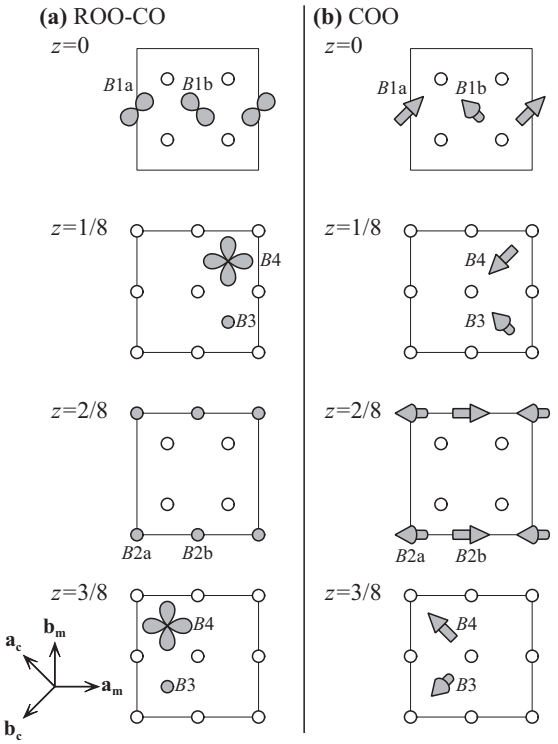


FIG. 1. Schematic representation of the real-number orbital and charge order (ROO-CO) in Refs. 28 and 29 (a) and the complex-number orbital order (COO) in Ref. 32 (b) on the $a_c/\sqrt{2} \times a_c/\sqrt{2} \times 2a_c$ cell with the $P2/c$ symmetry with a $Pmca$ constraint (Ref. 10). The alignments of the charges and orbitals for ROO-CO (a) and the directions of the orbital moments for COO (b) are shown for each layer parallel to the $a_m$-$b_m$ plane at $z = 0, 1/8, 2/8$, and $3/8$. The alignments on the other layers with $z > 3/8$ can be obtained with the symmetry operation $\{\Theta\sigma_b|\frac{\boldsymbol{c}_m}{2}\}$, where $\Theta$ stands for the time-reversal operator. The open circles denote oxygen atoms. In (a), the shaded circles represent $Fe^{3+}$ ions on $B$ sites, and the shaded figures at the $B1a$, $B1b$, and $B4$ sites symbolize $Fe^{2+}$ ions with dominantly occupied $YZ$, $ZX$, and $XY$ orbitals (in cubic notation) with the minority spin, respectively. In (b), the directions of the orbital magnetic moments are depicted by the arrows; more detailed information on the orbital polarization in each $B$ site for the COO state can be found in Table I.

this paper, the coordinates for the cubic lattice are represented with capital letters whereas those for the monoclinic lattice with small letters). With this ordering an insulating gap opens. In spite of large differences in the occupation numbers of the minority-spin $t_{2g}$ orbitals between the "$Fe^{2+}$" and "$Fe^{3+}$" sites ($\delta n_{t2g} \sim 0.7$), $e_g$ electrons compensate this differences resulting in rather small charge disproportion among the $B$ sites $\delta n \sim 0.23$, which is consistent with experiments.[30] Another orbital and charge order in the $Cc$ cell has been found to be most stable in a generalized gradient approximation with Hubbard $U$ (GGA + $U$) method with lattice structural optimization study.[31]

Although this real-number orbital and charge ordering (ROO-CO) seems to be widely accepted as the explanation of the Verwey transition, an alternative theory with complex-number orbital ordered (COO) state has been put forward using a spinless three-band Hubbard model.[32] In this COO state, ordered orbital $|\psi_l\rangle$ in each of the $B$ sites $l$ is described by a linear combination of the wave functions of the $t_{2g}$ orbitals with complex-number coefficients $C_{YZ}^{(l)}$, $C_{ZX}^{(l)}$, and $C_{XY}^{(l)}$ as

$$|\psi_l\rangle = C_{YZ}^{(l)}|YZ\rangle + C_{ZX}^{(l)}|ZX\rangle + C_{XY}^{(l)}|XY\rangle. \quad (1)$$

(The values of the coefficients and the properties of the COO state obtained with the pseudo-$Pmca$ lattice structure[10] are listed in Table I.) The formation of the COO state spontaneously breaks the time-reversal symmetry within the orbital degree of freedom, and as a result, noncollinear orbital moments $\sim 0.5\,\mu_B$ are induced on the $B$ sites [see Fig. 1(b)]. We note that since the orbital moments are aligned noncollinearly, the net orbital magnetization per $B$ site could be rather small. In contrast to the ROO-CO state, charge order is not a fundamental ingredient of the COO state, and charge disproportion is small even among the $t_{2g}$ orbitals (at most the difference is $\delta n_{t2g} \sim 0.2$). In this theory, a COO state with short-range order above $T_V$ is expected to develop into this COO state with long-range order coupled with the monoclinic lattice distortion below $T_V$.

Because of its site selectivity, resonant x-ray diffraction (RXD) is a useful tool to investigate systems with multiple sites. Particularly, by measuring the light polarization, azimuth angle of the scattering plane, and photon energy dependence of the reflection intensities, one can obtain information on local symmetry, valence state, or magnetic state of the specific sites.[33] However, observing charge or orbital order by RXD is not always straightforward, since the effects of lattice distortions associated with the ordering are often much stronger than those of the ordering.[34,35] On the other hand, since the $2p \rightarrow 3d$ dipole excitation occurs to its intermediate state, RXD at the transition-metal $L_{2,3}$ edges is expected to provide more direct information on the $3d$ electronic state of transition-metal compounds[36] and has been applied among other systems[37–41] also to magnetite. In this connection, the origin of the $(00\frac{1}{2})_c$ superstructure reflection (in the cubic notation) at the Fe $L_{2,3}$ resonance below $T_V$ has been disputed. Some authors have claimed that this reflection arises from not the orbital and charge order but from the lattice distortion concomitant with the ordering.[42–44] Through a series of works on the $(00\frac{1}{2})_c$ and $(001)_c$ reflections at the Fe $L_{2,3}$ resonance of $Fe_3O_4$, we have found that these reflections, indeed, contain direct information on the orbital and charge order below $T_V$.[45–47] There is also a study of the $(00\frac{1}{2})_c$ reflection at the O $K$ resonance with O $1s \rightarrow 2p$ excitation and this reflection has been interpreted as a signature of a particular charge and orbital order at the oxygen site.[48]

In a previous work[47] we investigated the azimuth angle and polarization dependence of the $(00\frac{1}{2})_c$ and $(001)_c$ reflections at the Fe $L_{2,3}$ resonance using a thin layer of magnetite partially detwinned by epitaxial growth on a stepped MgO(001) substrate. From azimuth and polarization analysis of the $(00\frac{1}{2})_c$ reflection intensities, the order in the $3d$ electronic state below $T_V$ was found to have a large monoclinic deformation. In most of the theories so far proposed on the Verwey transition, e.g., those in Refs. 24,26, and 27, the charge or orbital orders expected below $T_V$ are those with the orthorhombic symmetry or at most with small monoclinic deformations and therefore our finding imposes a strict limit on the candidates of the order below $T_V$.

TABLE I. Properties of the COO state with $P2/\underline{c}$ symmetry calculated with a spinless three-band Hubbard model (Ref. 32). The $X$, $Y$, and $Z$ components of orbital magnetic moment and its size $|\boldsymbol{m}_L|$ are shown in units of $\mu_B$ for each of six nonequivalent $B$ sites in the $P2/c$ cell together with the occupation numbers of the minority-spin $YZ$, $ZX$, and $XY$ orbitals and their total $n_{t2g}$ ($\equiv n_{YZ}+n_{ZX}+n_{XY}$). The $YZ$, $ZX$, and $XY$ components of the maximally occupied orbital $|\psi\rangle = C_{YZ}|YZ\rangle + C_{ZX}|ZX\rangle + C_{XY}|XY\rangle$ of the minority-spin $t_{2g}$ orbital and their occupation number $n_{\max}$ are also listed for each $B$ site. For the alignment of the orbital magnetic moments, see also Fig. 1(b).

| | $B1a$ ($z=0$) | $B1b$ ($z=0$) | $B2a$ ($z=1/4$) | $B2b$ ($z=1/4$) | $B3$ ($z\sim 3/8$) | $B4$ ($z\sim 3/8$) |
|---|---|---|---|---|---|---|
| $(m_L)_X$ | −0.087 | 0.125 | 0.227 | −0.357 | −0.025 | 0.499 |
| $(m_L)_Y$ | −0.540 | 0.014 | 0.227 | −0.357 | 0.337 | −0.040 |
| $(m_L)_Z$ | 0.083 | 0.272 | 0.359 | −0.104 | 0.195 | 0.094 |
| $\|\boldsymbol{m}_L\|$ | 0.553 | 0.299 | 0.482 | 0.516 | 0.390 | 0.509 |
| $n_{YZ}$ | 0.367 | 0.065 | 0.194 | 0.122 | 0.279 | 0.014 |
| $n_{ZX}$ | 0.013 | 0.335 | 0.194 | 0.122 | 0.049 | 0.245 |
| $n_{XY}$ | 0.234 | 0.015 | 0.104 | 0.292 | 0.110 | 0.276 |
| $n_{t2g}$ | 0.613 | 0.416 | 0.492 | 0.535 | 0.437 | 0.535 |
| $C_{YZ}$ | 0.776 | −0.377 | −0.630 | −0.474 | −0.813 | −0.131 |
| $C_{ZX}$ | $-0.096+0.086i$ | $0.034-0.910i$ | $0.220-0.590i$ | $0.426+0.208i$ | $-0.088-0.286i$ | $-0.143-0.665i$ |
| $C_{XY}$ | $0.217+0.578i$ | $0.166+0.038i$ | $0.259+0.373i$ | $0.167-0.723i$ | $0.043+0.497i$ | $0.651-0.311i$ |
| $n_{\max}$ | 0.606 | 0.403 | 0.483 | 0.526 | 0.420 | 0.527 |

The purpose of this paper is to discuss the energy dependence of the $(00\frac{1}{2})_c$ and $(001)_c$ diffraction intensities quantitatively and to demonstrate to what extent the resonance spectra are affected by the degree and kind of the monoclinic deformation of the order using a configuration-interaction $FeO_6$ cluster model. To this end, we compare experimental data with theoretical spectra for ROO-CO states with pseudo-$Pmca$ and $Cc$ symmetries predicted by the band structure theories in Refs. 28–31 and for the COO state with a large monoclinic deformation in Ref. 32. The effects of the lattice distortions on the $(00\frac{1}{2})_c$ reflection intensities and charge disproportionation on the $(001)_c$ reflection intensities are also discussed.

## II. EXPERIMENTAL METHODS

### A. Film growth

$Fe_3O_4$ thin films were epitaxially grown on epi-polished MgO(001) substrates using the molecular beam epitaxy (MBE) technique. The base pressure of the growth chamber was in the low $10^{-10}$ mbar range. MgO crystals were chosen as substrates because of the very small lattice mismatch of 0.3% between MgO and $Fe_3O_4$, with lattice constants of 4.212 and 8.396 Å, respectively. Flat substrates as well as substrates with a 6° miscut towards [010] were used (see below). Before the film growth, MgO(001) substrates were annealed at around 873 K in an oxygen atmosphere of $\simeq 3\times 10^{-7}$ mbar for 2 hours in order to remove contaminants such as hydrocarbons.[49] The $Fe_3O_4$ thin films were epitaxially grown on the well-annealed MgO(001) substrate at 523 K in an oxygen atmosphere of $\simeq 3\times 10^{-7}$ mbar.[46,50,63] The surface evolution of $Fe_3O_4$ thin films was real-time monitored *in situ* by reflection high energy electron diffraction (RHEED). The thickness of the films was determined from the intensity oscillation of the RHEED specular beam. Typical growth rates were about 72 seconds per monolayer. The sharp RHEED patterns and clear oscillations during the whole growing process reveal a layer-by-layer growth mode.[51–53]

### B. RSXD measurement

The resonant soft x-ray diffraction (RSXD) experiments were performed at the beam lines UE52-SGM and UE46-PGM-1 of the electron storage ring BESSY II operated by the Helmholtz-Zentrum Berlin (HZB). Part of the data were acquired using the two-circle UHV diffractometer designed at the Freie Universität Berlin, part of them with a UHV diffractometer designed at the University of Cologne. The geometry of the experiment is shown in Fig. 2. The polarization of incoming light was either perpendicular ($\sigma$ polarization) or parallel ($\pi$ polarization) to the scattering plane. A silicon-diode photon detector without polarization analysis was used with the angular acceptance set to 1° in the scattering plane and 5° perpendicular to it. For the azimuth-dependent study of the scattering intensity, the sample is rotated around the scattering vector $\boldsymbol{q}=\boldsymbol{k}'-\boldsymbol{k}$, with $\boldsymbol{k}$ ($\boldsymbol{k}'$) being the wave vector of the incoming (outgoing) photon. $\phi$ denotes an azimuthal angle.

For the experiments we used 40 nm thick magnetite films. The photon energy dependence spectra were recorded by varying the photon energy and keeping the momentum transfer constant.[46] Since the $(001)_c$ peak maximum cannot be reached

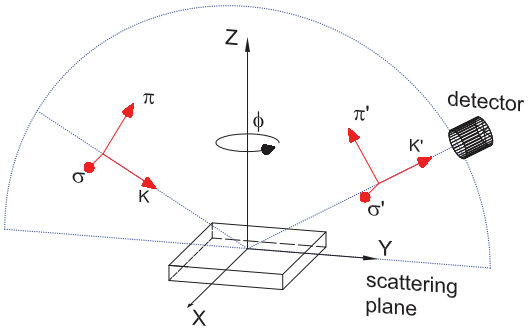


FIG. 2. (Color online) The geometric arrangement in our RSXD experiment. The polarization of incoming light was either perpendicular ($\sigma$ polarization) or parallel ($\pi$ polarization) to the scattering plane.

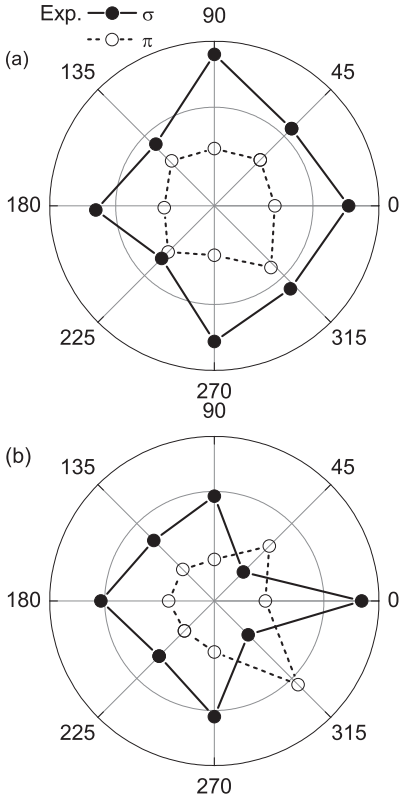


FIG. 3. The azimuthal-dependent polar plot of the RSXD $L_3$ maxima intensity of the $(00\frac{1}{2})_c$ reflection for $\sigma$ (filled circle) and $\pi$ (open circle) polarized light taken from (a) a full-twinned $Fe_3O_4$ thin film grown on a flat MgO substrate and (b) a partially untwinned $Fe_3O_4$ thin film grown on a stepped MgO substrate at 83 K below $T_V$.

at the Fe-$L_3$ resonance the resonance spectra for the (001) peak were recorded at $L = 0.95$.[45]

## III. EXPERIMENTAL RESULTS

Figure 3(a) shows the polar plot of the $L_3$ maximum intensity of the $(00\frac{1}{2})_c$ diffraction peak from a $Fe_3O_4$ film grown on a flat MgO substrate taken at 83 K. Filled and open symbols are $\sigma$- and $\pi$-polarized incoming light, respectively; lines are for eye guidance. The azimuthal angle $\phi$ is defined to be zero when the scattering plane is parallel to one of the cubic axes. It shows a clear dependence of the scattering intensity on the polarization and the sample azimuthal angle. The pattern shows two slightly distorted squares rotated by 45° with respect to each other. The reason for this fourfold symmetry is that during the transition from the high-temperature cubic to the low-temperature monoclinic phase a multiple twinning of the crystal occurs. For the films we find only twins with the $c$ axis pointing out of the film plane. For this direction of $c$ there remain four possible directions for $a$ and $b$. Therefore, the pattern reflects a fourfold twinning with almost equal domain ratios for our film.[47] Twinning can be further reduced by growing the films on MgO substrates, which have a surface normal that was tilted by 6° away from [001] towards [010] using an otherwise identical growth procedure. Additional epitaxial strain caused by the step edges[54,55] leaves only two out of four possible domains to form with their monoclinic $a_m$ axis rotated by ± 45° from the mirror plane spanned by the 0°/180° azimuth and the $[001]_c$ direction. Here, the azimuthal angle $\phi$ is defined to be zero when the wave vectors of the incoming and outgoing light are perpendicular to the step edges on MgO substrate and have positive components of descending direction of steps (see Fig. 4). Note that it is still an open question whether the $c_m$ axes of the domains in these partially detwinned samples are slanted toward or away from the step edges. The azimuthal dependence of the $L_3$ maximum intensity displayed in Fig. 3(b) shows a low-symmetry pattern, where the intensities are symmetric functions of $\phi$ with respect to $\phi = 0°$ but have no twofold or fourfold rotational symmetry.

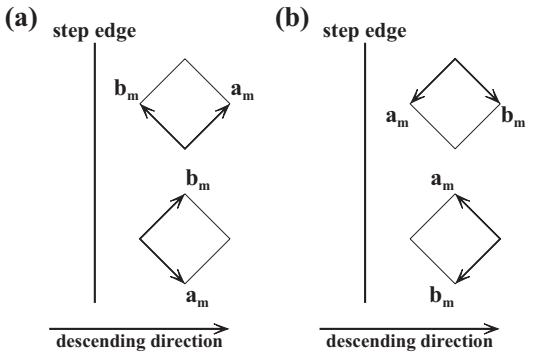


FIG. 4. Orientations of the monoclinic lattice coordinates of the domains in $Fe_3O_4$ thin film grown on a stepped MgO substrate. Two possible ways of partial detwining are indicated, where two kinds of domains in which the $c_m$ axes of the monoclinic lattice are slanted toward (a) or away from (b) the step edges. Note that the lattice angle between the $a_m$ and $c_m$ axes is about $\beta = 90.236°$ (Ref. 10).

With this degree of untwinning the complexity of the system is largely reduced. The resonance spectra presented in Fig. 5(a) are considered to be the superposition of two different sample geometries, which can be well treated in the simulation. Most of the intensity of the spectra is in the main peak at the $L_3$ resonance (M). A pronounced shoulder (A) is visible on the low-energy side, while the high-energy shoulder (B) is mostly visible in the spectra obtained with $\pi$-polarized x-rays. The feature (C) is also part of the resonance of the specular reflectivity background below the $(00\frac{1}{2})$ diffraction peak[45] and its intensity is overestimated in the spectra without explicit background subtraction, while the background contribution to the other features is small.

Figure 5(b) shows the raw RSXD spectra of the $(001)_c$ reflection at the Fe $L_{2,3}$ edges for $\sigma$- and $\pi$-polarized light taken at $\phi = 0°$ and 83 K from a partially untwinned $Fe_3O_4$ thin film grown on a stepped MgO substrate. In contrast to the $(00\frac{1}{2})_c$ reflection, the $(001)_c$ diffraction peak gives only mild polarization dependence. By subtracting the specular reflectivity background as the procedure used in Ref. 45, we found that this mild polarization dependence of the $(001)_c$ reflection is negligible as shown in Fig. 12(a).

## IV. ANALYSIS OF THE REFLECTION INTENSITIES

### A. Symmetry consideration

Before dealing with the photon energy dependence of the intensities with the aid of a more rigorous cluster model, we

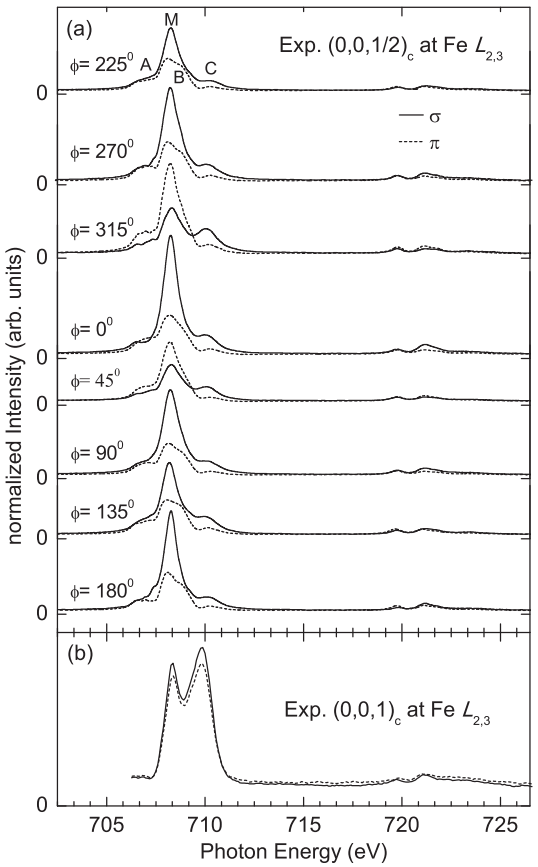


FIG. 5. The Fe $L_{2,3}$ edges RSXD spectra of (a) the $(00\frac{1}{2})_c$ reflection measured at various azimuthal angles $\phi$ and (b) the $(001)_c$ reflection at $\phi = 0^\circ$ from a partially untwinned $Fe_3O_4$ thin film grown on a stepped MgO substrate [the same data presented in Fig. 1(a) in Ref. 47]. The sample azimuth and polarization of light correspond to Fig. 3(b). The solid and dashed lines are $\sigma$- and $\pi$-polarized incoming light, respectively. All data were taken at 83 K.

will discuss the space-group symmetry of the electronic state in the low-temperature phase using a rather phenomenological model, where a single level is assumed in the intermediate state. This is an acceptable approximation since most of the spectral weight is concentrated in peak M. This section is an extension of the discussion in Ref. 47. The scattering amplitude of RXD within the $2p \rightarrow 3d$ electric dipole transition at the resonant maximum can be written as

$$A(\boldsymbol{\varepsilon},\boldsymbol{\varepsilon}') = i \sum_l \exp(i\boldsymbol{q}\cdot\boldsymbol{R}_l) \sum_{i,j} \varepsilon_i \varepsilon'_j f_{ij}^{(l)}, \tag{2}$$

where $f_{ij}^{(l)}$ represents the scattering tensor of site $l$ at the position $\boldsymbol{R}_l$ and $\boldsymbol{\varepsilon}$ and $\boldsymbol{\varepsilon}'$ denote the polarization vectors of the incident and scattering light, respectively. Within this single excitation-level approximation, the relations $f_{ij}^{(l)} = f_{ji}^{(l)*}$ hold at the resonant maximum.

It is also essential to consider the transformations of the magnetic moments on each Fe site by the symmetry operations, i.e., magnetic space group. This is not only so for the COO state, where large orbital moments are present on $B$ sites, but, in general, the scattering intensities at the $3d$ transition-metal $L_{2,3}$ edges are sensitive to the direction of the spin moments owing to the large spin-orbit interaction of the $2p$ core hole in the intermediate state.[33]

### 1. $(00\frac{1}{2})_c$ reflection

If the magnetization direction is along the $c_m$ axis (which is the easy axis[56]), and the $Pmca$ lattice structure is assumed, the symmetry of the low-temperature phase including the magnetic order is $P\underline{mc}a$. Using the same definition of the coordination for the atomic positions on the $a_c/\sqrt{2} \times a_c/\sqrt{2} \times 2a_c$ pseudo-$Pmca$ cell as in Ref. 10 and applying the symmetry operations in the $P\underline{mc}a$ space group $\{\sigma_c|\frac{\boldsymbol{a}_m}{2} + \frac{\boldsymbol{c}_m}{2}\}$, $\{\Theta\sigma_b|\frac{\boldsymbol{c}_m}{2}\}$, and $\{\Theta\sigma_a|\frac{\boldsymbol{a}_m}{2}\}$, where $\Theta$ denotes the time-reversal operator, the scattering amplitude of the $(00\frac{1}{2})_c$ reflection caused by the Fe ions on the $B$ sites can be expressed as

$$A(\boldsymbol{\varepsilon},\boldsymbol{\varepsilon}') \propto (\varepsilon_y\varepsilon'_z + \varepsilon_z\varepsilon'_y)\mathrm{Re}[F_{yz}] + i(\varepsilon_z\varepsilon'_x - \varepsilon_x\varepsilon'_z)\mathrm{Im}[F_{zx}] \tag{3}$$

with

$$F_{ij} = 4\left(f_{ij}^{(1)} + \cos 2\pi z_3 f_{ij}^{(3)} + \cos 2\pi z_4 f_{ij}^{(4)}\right).$$

Here, $z_3$ and $z_4$ are the $z$ coordinates of the $B3$ and $B4$ sites, respectively, with values of approximately 3/8. The $B1a$ and $B1b$ sites as well as the $B2a$ and $B2b$ sites are crystallographically equivalent within $Pmca$ (see Fig. 1). The $B2$ sites do not contribute to the scattering amplitude, and terms with the real parts of $f_{yz}^{(l)}$ and the imaginary parts of $f_{zx}^{(l)}$ of each site other than $B2$ remain. If the magnetic order is not considered, i.e., the $Pmca$ symmetry, the term with the imaginary parts of $f_{zx}^{(l)}$ further vanishes.

If monoclinic $P2/c$ distortions are considered, the symmetry of the system having the magnetization direction perpendicular to the $b_m$ axis is lowered to $P\underline{2}/\underline{c}$, where the $\sigma_a$ mirror plane is now removed and symmetry operations $\{\Theta\sigma_b|\frac{\boldsymbol{c}_m}{2}\}$ and $\{\Theta C_2|\frac{\boldsymbol{c}_m}{2}\}$ are retained. This symmetry is the same to the COO state in Ref. 32. The scattering amplitude of the $(00\frac{1}{2})_c$ reflection is then written as

$$\begin{aligned} A(\boldsymbol{\varepsilon},\boldsymbol{\varepsilon}') \propto{}& (\varepsilon_y\varepsilon'_z + \varepsilon_z\varepsilon'_y)\mathrm{Re}[F_{yz}] + i(\varepsilon_z\varepsilon'_x - \varepsilon_x\varepsilon'_z)\mathrm{Im}[F_{zx}] \\ &+ (\varepsilon_x\varepsilon'_y + \varepsilon_y\varepsilon'_x)\mathrm{Re}[F_{xy}] \end{aligned} \tag{4}$$

with

$$F_{ij} = 2\left(f_{ij}^{(1a)} + f_{ij}^{(1b)}\right) + 4\cos 2\pi z_3 f_{ij}^{(3)} + 4\cos 2\pi z_4 f_{ij}^{(4)}.$$

The real parts of $f_{xy}^{(l)}$ now appear in the expression.

In the reference frame of the experiment (Fig. 2) the intensities with the $\sigma$-polarized ($\mu = \sigma$) and $\pi$-polarized ($\mu = \pi$) incident light at the resonant maximum are described as

$$I_\mu(\phi_\mathrm{m}) = |A(\boldsymbol{\varepsilon}_\mu,\boldsymbol{\varepsilon}'_\sigma)|^2 + |A(\boldsymbol{\varepsilon}_\mu,\boldsymbol{\varepsilon}'_\pi)|^2, \tag{5}$$

where

$$\left.\begin{aligned} \boldsymbol{\varepsilon}_\sigma &= \boldsymbol{\varepsilon}'_\sigma = (-\sin\phi_\mathrm{m}, \cos\phi_\mathrm{m}, 0) \\ \boldsymbol{\varepsilon}_\pi &= (\cos\phi_\mathrm{m}\sin\theta, \sin\phi_\mathrm{m}\sin\theta, \cos\theta) \\ \boldsymbol{\varepsilon}'_\pi &= (-\cos\phi_\mathrm{m}\sin\theta, -\sin\phi_\mathrm{m}\sin\theta, \cos\theta) \end{aligned}\right\} \tag{6}$$

and $\theta \approx 31.3^\circ$ represents the Bragg angle; $\phi_\mathrm{m}$ denotes the azimuth angle and is $\phi_\mathrm{m} = 0$ when the scattering plane is parallel to the $x$ axis ($a_\mathrm{m}$ axis).

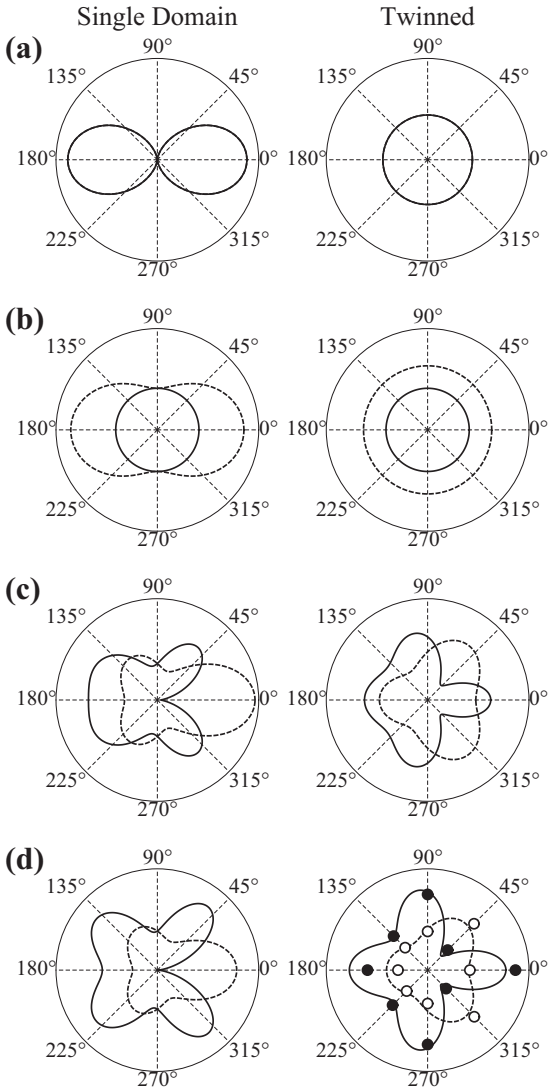


FIG. 6. Polar plots of theoretical azimuth and polarization dependence of the $(00\frac{1}{2})_c$ reflection intensities. The solid and dashed lines denote the intensities with the $\sigma$- and $\pi$-polarization light, respectively. Those for the single-domain crystal (on the left) and for the $Fe_3O_4$ layer on the stepped MgO substrate (on the right) are drawn. The choices of the three components of the scattering matrices in (a) and (b) are for $Pmca$, and those in (c) are for $P2/c$; their ratios are in (a), $\mathrm{Re}[F_{yz}] : \mathrm{Im}[F_{zx}] : \mathrm{Re}[F_{xy}] = 1 : 0 : 0$, in (b), $1 : 1 : 0$ and in (c), $1 : 1 : 1$. In (d), theoretical intensities obtained with $\mathrm{Re}[F_{yz}] : \mathrm{Im}[F_{zx}] : \mathrm{Re}[F_{xy}] = 1.0 : 1.4 : 2.0$ are compared with experimental integrated intensity of $L$ scan at Fe $L_3$ maximum of the $Fe_3O_4$ layer on the stepped MgO substrate with $\sigma$ ($\pi$) polarized light in Ref. 47 depicted as closed (open) circles.

To examine how the differences in the symmetry affect the azimuth and polarization dependence of the scattering intensities, in Fig. 6 polar plots of $I_\mu(\phi)$ calculated using Eq. (4) are shown with solid ($I_\sigma$) and dashed ($I_\pi$) lines. Those obtained with three different sets of the scattering matrices $\mathrm{Re}[F_{yz}]$, $\mathrm{Im}[F_{zx}]$, and $\mathrm{Re}[F_{xy}]$ in Eq. (4) are drawn: (a) and (b) for $Pmca$ and (c) for $P2/c$. In the left column of Fig. 6, those for the single-domain crystal are shown; in the right column, those for the $Fe_3O_4$ layer on the stepped MgO surface are depicted, where two crystal domains are rotated by $\pm 45^\circ$ around the $z$ axis and where two directions of the magnetization $\pm\boldsymbol{M}$ are assumed to coexist with the same volume fraction:

$$\overline{I}_\mu(\phi) = \tfrac{1}{4}[I_\mu(\phi + 45^\circ) + I_\mu(\phi - 45^\circ) + I_\mu(-\phi + 45^\circ) + I_\mu(-\phi - 45^\circ)]. \quad (7)$$

[Note that because of $\{\Theta\sigma_b|\frac{\boldsymbol{c}_m}{2}\}$ symmetry, there is a relation $\Theta I_\mu(\phi) = \sigma_b I_\mu(\phi) = I_\mu(-\phi)$.] This corresponds to the partial detwining shown in Fig. 4(a). The shapes of the intensity curves in (a) and (b) corresponding to $Pmca$ are centrosymmetric owing to the $\sigma_a$ and $\sigma_b$ mirror symmetries. In contrast, the removal of the $\sigma_a$ mirror makes those for $P2/c$ (c) noncentrosymmetric. The differences are particularly evident for the intensity curves for the twinned crystal indicated in the right column in Fig. 6. While those for $Pmca$ have no angular dependence, the intensities for $P2/c$ have prominent polarization and angular dependence and agree well with the experimental $L_3$ maximum intensities in Fig. 3(b). To obtain the same degree of noncentrosymmetric shape in (c), the value of $\mathrm{Re}[F_{xy}]$ must be comparable to the other two scattering components.

For simplicity, in the above discussions on the intensity curves it is assumed that symmetry lowering occurs within the $a_c/\sqrt{2} \times a_c/\sqrt{2} \times 2a_c$ supercell. However, the discussions can be generalized to the monoclinic $Cc$ symmetry with the $\sqrt{2}a_c \times \sqrt{2}a_c \times 2a_c$ supercell. The scattering amplitude for the $Cc$ symmetry, where only the symmetry operation $\{\Theta\sigma_b|\frac{\boldsymbol{c}_m}{2}\}$ is retained, can be written assuming the same coordination system and definition of 16 $B$ sites ($B1 \sim B16$) in Ref. 31:

$$\begin{aligned} A(\boldsymbol{\varepsilon},\boldsymbol{\varepsilon}') \propto\ & (\varepsilon_y\varepsilon'_z + \varepsilon_z\varepsilon'_y)\{\mathrm{Re}[F^{\mathrm{S}}_{yz}] + i\mathrm{Re}[F^{\mathrm{A}}_{yz}]\} \\ & + i(\varepsilon_z\varepsilon'_x - \varepsilon_x\varepsilon'_z)\{\mathrm{Im}[F^{\mathrm{S}}_{zx}] + i\mathrm{Im}[F^{\mathrm{A}}_{zx}]\} \\ & + (\varepsilon_x\varepsilon'_y + \varepsilon_y\varepsilon'_x)\{\mathrm{Re}[F^{\mathrm{S}}_{xy}] + i\mathrm{Re}[F^{\mathrm{A}}_{xy}]\} \end{aligned} \quad (8)$$

with

$$F^{\mathrm{S}}_{ij} = 2\sum_{l=1}^{16} \cos 2\pi z_l f^{(l)}_{ij},$$

$$F^{\mathrm{A}}_{ij} = 2\sum_{l=1}^{16} \sin 2\pi z_l f^{(l)}_{ij}.$$

Note that for the $C2/c$ symmetry, all the terms with $F^{\mathrm{A}}_{ij}$ vanish. It is easy to show from Eqs. (5)–(8) that if the orthorhombic $Cmc2_1$ symmetry is assumed, which corresponds to setting the terms with $\mathrm{Re}[F^{\mathrm{S,A}}_{xy}]$ to zero in Eq. (8), there is no angular dependence of the intensities for the twinned crystal.

These results show that the experimental angular dependence of the intensities of $(00\frac{1}{2})_c$ reflection in $Fe_3O_4$ below $T_V$ cannot be explained with an orthorhombic symmetry and thus monoclinic distortion should be large. On the other hand, the monoclinic distortion of the lattice below $T_V$ is known to be small, and its atomic positions can be well described within the structure model with the $Pmca$ symmetry.[9,10] As discussed in one of our previous works,[47] this discrepancy in the degree of the monoclinic distortions between the lattice and what was observed in the RXD experiments indicates that the azimuth

and polarization dependence of RXD is particularly sensitive to the $3d$ electronic state, and the orbital (or simultaneous orbital and charge) order in the $3d$ electronic state below $T_V$ should have a large monoclinic deformation.

It is worthwhile to notice that the conditions $f_{ij}^{(l)} = f_{ji}^{(l)*}$, which hold only for the single-level model assumed here, oversimplify the situations with magnetized samples. In general, the dissipative term $\Gamma$ in Eq. (13) breaks the time-reversal symmetry of propagation of light. As a result, symmetries with $\Theta$ are lost. For example, $\Theta\sigma_a$ and $\Theta\sigma_b$ symmetries expected with $P\underline{m}c\underline{a}$ as in the single-domain case in Fig. 6(b) are removed and only $C_2$ ($= \Theta\sigma_a\Theta\sigma_b$) symmetry remains as found in the polar plot in Fig. 7(b) obtained with the cluster model calculations.

#### 2. $(001)_c$ *reflection*

The photon wavelengths at the Fe $L_{2,3}$ resonances are slightly too long to satisfy the Bragg condition of the $(001)_c$ reflection. For the thin layer of magnetite, however, this peak is broadened along the (001) direction of reciprocal space due to the finite thickness of the sample and therefore measurements are possible at the tail of the peak which is reachable in reciprocal space.[45] The amplitude of the $(001)_c$ reflection for the $P\underline{2}/\underline{c}$ symmetry can be written as

$$\begin{aligned} A(\boldsymbol{\varepsilon},\boldsymbol{\varepsilon}') \propto\ & \varepsilon_x\varepsilon'_x F_{xx} + \varepsilon_y\varepsilon'_y F_{yy} + \varepsilon_z\varepsilon'_z F_{zz} \\ & + i(\varepsilon_y\varepsilon'_z - \varepsilon_z\varepsilon'_y)\mathrm{Im}[F_{yz}] + (\varepsilon_z\varepsilon'_x + \varepsilon_x\varepsilon'_z)\mathrm{Re}[F_{zx}] \\ & + i(\varepsilon_x\varepsilon'_y - \varepsilon_y\varepsilon'_x)\mathrm{Im}[F_{xy}] \end{aligned} \tag{9}$$

with

$$\begin{aligned} F_{ij} = {} & 2\left(f_{ij}^{(1a)} + f_{ij}^{(1b)}\right) - 2\left(f_{ij}^{(2a)} + f_{ij}^{(2b)}\right) \\ & + 4\cos 4\pi z_3 f_{ij}^{(3)} + 4\cos 4\pi z_4 f_{ij}^{(4)}. \end{aligned}$$

Not only the off-diagonal components but the diagonal components ($F_{xx}$, $F_{yy}$, and $F_{zz}$) of the scattering matrices contribute to this reflection. Since the phase factors $\cos 4\pi z_{3,4}$ for the $B3$ and $B4$ sites are small $|\cos 4\pi z_{3,4}| < 0.1$, differences between the scattering factors of the $B1$ and $B2$ sites mostly affect the reflection. With the experimental condition $\theta \sim \pi/2$, only the terms with $F_{xx}$, $F_{yy}$, and $\mathrm{Im}[F_{xy}]$ remain. The intensities for the thin layer of magnetite on MgO substrate are therefore expected to have no azimuth or polarization dependence:

$$I_\sigma(\phi) = I_\pi(\phi) \propto F_{xx}^2 + F_{yy}^2 + \tfrac{1}{2}(\mathrm{Im}[F_{xy}])^2. \tag{10}$$

### B. Cluster model

So far we have discussed the symmetry of the $3d$ electronic state of $Fe_3O_4$ below $T_V$ using a phenomenological model. However, to verify whether any of the orbital and charge orders so far proposed for $Fe_3O_4$ is compatible with the experiments, a microscopic model capable of describing both the $3d$ state in the initial state and the excitation levels (multiplets) quantitatively is required. In this subsection, we will therefore present theoretical $(00\frac{1}{2})_c$ and $(001)_c$ reflection intensities obtained with a configuration-interaction $FeO_6$ cluster model.[41,57,59] Three kinds of orbital orders (two ROOCOs and one COO) are considered as the initial state in the calculations and the symmetry and other aspects of the orders including the effects of lattice distortions will be discussed by comparison with the experimental intensities.

#### 1. *General description of the model*

To describe the electronic state of magnetite, for each of the $B$ sites an $FeO_6$ octahedral cluster is used, in which the $3d$ orbitals on the site and the $2p$ orbitals of the surrounding six oxygen atoms are taken into account.[57] Because of strong hybridization between the Fe $3d$ and O $2p$ orbitals, the "$Fe^{2+}$ ion" corresponding to an $[FeO_6]^{10-}$ cluster cannot be regarded as a pure ionic state but is described as a superposition of states with the $3d^6$, $3d^7\underline{L}$, and $3d^8\underline{L}^2$ electronic configurations, where $\underline{L}$ denotes a hole on the ligand. Similarly, the "$Fe^{3+}$ ion" corresponding to $[FeO_6]^{9-}$ is expressed as a superposition of states with the $3d^5$, $3d^6\underline{L}$, $3d^7\underline{L}^2$, and $3d^8\underline{L}^3$ configurations. The $3d$ and minority-spin $t_{2g}$ electron occupations of the $Fe^{2+}$ state in our model are $n = 6.15$ and $n_{t2g} = 1.03$, respectively, and those for the $Fe^{3+}$ state are $n = 5.45$ and $n_{t2g} = 0.13$. The differences in $n$ and $n_{t2g}$ between the $Fe^{2+}$ and $Fe^{3+}$ states are $\delta n \sim 0.7$ and $\delta n_{t2g} \sim 0.9$ and $\delta n$ is substantially reduced from the pure ion value even without considering the effects of electron hopping between the $B$ sites.

The valence fluctuation caused by electron hopping between $B$ sites is approximated by assuming that each of the initial states of the $B$ sites is described as a mixture of $Fe^{2+}$ and $Fe^{3+}$ states. Such a state can be written as a density matrix $\rho_l$ constructed from the ground-state wave functions $\Psi_l^{(2+)}$ of the $[FeO_6]^{10-}$ cluster and $\Psi_l^{(3+)}$ of the $[FeO_6]^{9-}$ cluster as

$$\rho_l = w_l^{(2+)}\left|\Psi_l^{(2+)}\right\rangle\left\langle\Psi_l^{(2+)}\right| + w_l^{(3+)}\left|\Psi_l^{(3+)}\right\rangle\left\langle\Psi_l^{(3+)}\right|, \tag{11}$$

where $w_l^{(2+)}$ ($w_l^{(3+)}$) is the probability of the $Fe^{2+}$ ($Fe^{3+}$) state occurring at site $l$ and $w_l^{(2+)} + w_l^{(3+)} = 1$. These probabilities $w_l^v$ are chosen so as to reproduce a charge order assumed in the initial state.

The $3d$-$3d$ Coulomb and exchange interactions (full multiplets), hybridization between the $3d$ and O $2p$ orbitals, a crystal field, the $3d$ spin-orbit interaction, and a molecular field induced by the ferrimagnetic order are considered in the initial state. For the intermediate state, the considered configurations reached by the Fe $2p \rightarrow 3d$ electronic dipole transition from the initial state are $2\underline{p}3d^7$, $2\underline{p}3d^8\underline{L}$, and $2\underline{p}3d^9\underline{L}^2$ for the $Fe^{2+}$ states and $2\underline{p}3d^6$, $2\underline{p}3d^7\underline{L}$, $2\underline{p}3d^8\underline{L}^2$, and $2\underline{p}3d^9\underline{L}^3$ for the $Fe^{3+}$ states, where $2\underline{p}$ denotes the Fe $2p$ core hole. In the intermediate state, in addition to the above interaction, the Coulomb and exchange interaction between the Fe $2p$ core hole and $3d$ electrons and the spin-orbit interaction of the $2p$ core hole are included. A detailed description of the cluster model can be found in Ref. 57.

Lattice deformations affect the RSXD signal in two ways: one is those through the modification of the hybridization strength and crystal field due to the displacements of the surrounding oxygen atoms relative to the site and, the other is via changes in the phase factors $\exp(i\boldsymbol{q}\cdot\boldsymbol{R}_l)$ owing to the displacement of the site itself. For the former, the hopping matrix between the $3d$ and O $2p$ orbitals $V^{(l)}$ are parametrized with the Slater-Koster parameters $pd\sigma$ and $pd\pi$ and the Fe-O bond length $R$ dependence $pdm \propto 1/R^{7/2}$ is assumed after

Harrison.[58] To ease computational workload, only a part of the ligand O $2p$ bases which is strongly hybridized with the $3d$ state is included in the calculations as described in the Appendix.

The so-called crystal field is in reality a sum of the electrostatic field from surrounding ions and the energy shift caused by the nonorthogonality between the $3d$ and oxygen $2p$ orbitals. The latter is $-(V^{(l)}S^{\dagger} + SV^{(l)\dagger})$ for a small overlap integral $S$. Instead of including both the effects, assuming $S \propto V^{(l)}$ and introducing an empirical parameter $r_{\rm Q}$, we rewrite the contribution of the six neighboring oxygen ions approximately as $r_{\rm Q}V^{(l)}V^{(l)\dagger}$. For the contribution from the rest of ions, those other than the Fe ion and neighboring oxygen ions in an $FeO_6$ cluster, effects of the monoclinic distortion are omitted, and only a trigonal field is assumed (the $B$ sites have the $D_{3d}$ symmetry in the cubic phase with their trigonal axes along one of the $\langle 111\rangle_{\rm c}$ directions). The crystal field is then written as

$$H^{(l)}_{\rm cryst} = r_{\rm Q}V^{(l)}V^{(l)\dagger} + D_{\rm trg}\left(\tfrac{1}{3}P_{t2g} - \left|a^{(l)}_{1g}\right\rangle\left\langle a^{(l)}_{1g}\right|\right), \qquad (12)$$

where $D_{\rm trg} = \varepsilon(e^{\pi}_g) - \varepsilon(a_{1g})$ is the energy difference between the $e^{\pi}_g$ and $a_{1g}$ levels of the $t_{2g}$ orbital, $P_{t2g}$ denotes the projection operator of the $t_{2g}$ orbitals, and $|a_{1g}\rangle$ is defined with a unit vector $\boldsymbol{\alpha}^{(l)}$ parallel to the pseudotrigonal axis of site $l$ as

$$\left|a^{(l)}_{1g}\right\rangle = \alpha^{(l)}_X|YZ\rangle + \alpha^{(l)}_Y|ZX\rangle + \alpha^{(l)}_Z|XY\rangle.$$

The scattering factor of site $l$ is described as

$$f_l(\boldsymbol{\varepsilon},\boldsymbol{\varepsilon}',\omega) \propto \sum_v w^v_l\left\langle\Psi^v_l\right|\boldsymbol{\varepsilon}\cdot\boldsymbol{r} \times \frac{\omega^2}{E^v_l + \hbar\omega - H_l - {\rm i}\Gamma(\omega)}\boldsymbol{\varepsilon}'\cdot\boldsymbol{r}\left|\Psi^v_l\right\rangle, \qquad (13)$$

where $v\,(=2+$ or $3+)$ is the valence, and $\omega$, $E^v_l$, $H_l$, and $\Gamma$ represent the incident photon energy, the eigenvalue of the ground state with $v$, the intermediate state Hamiltonian, and the imaginary part of the self-energy, respectively. The intensity of the scattering as a function of $\omega$ and the azimuth angle $\phi$ is

$$I_{\mu}(\omega,\phi) = \sum_{\nu}\left|\sum_l \exp(i\boldsymbol{q}\cdot\boldsymbol{R}_l)f_l(\boldsymbol{\varepsilon}_{\mu},\boldsymbol{\varepsilon}'_{\nu},\omega)\right|^2, \qquad (14)$$

where $\nu$ and $\mu$ represent the $\sigma$- or $\pi$-polarization of the incident and scattering light in Eq. (6).

The values of the parameters adopted are the on-site Coulomb energy of $3d$ electrons $U_{dd} = 6.0$ eV, the core-hole potential energy $U_{dc} = 7.5$ eV, the charge transfer energies for the $Fe^{2+}$ states $\Delta_{2+} = 7.0$ eV and for the $Fe^{3+}$ states $\Delta_{3+}$ $(= \Delta_{2+} - U_{dd}) = 1.0$ eV, and the O $2p$-$2p$ hopping integral $T_{pp}\,(= pp\pi - pp\sigma) = 0.7$ eV. The value of the Fe $3d$–O $2p$ hopping integral is $pd\sigma = -1.21$ eV at Fe-O distance 2.15 Å and a relation $pd\pi = -0.433\,pd\sigma$ is assumed. For the crystal field, $r_{\rm Q} = 0.15\ ({\rm eV})^{-1}$ is chosen so that the average of $10Dq$ over $B$ sites is $10Dq \sim 0.7$ eV. The parameter set employed in this study is essentially the same as that determined from analysis of the resonant photoemission experiments with circular polarized light using the similar cluster model[59] except that the variation of hopping integrals owing to monoclinic distortions is considered in the present work. For example, if we assume the pseudo-$Pmca$ lattice structure in Ref. 10, the values of $pd\pi$'s for the shortest (1.964 Å) and longest (2.116 Å) Fe-O bonds among $B$ sites are 0.72 and 0.55 eV, respectively, and the difference of the two is 27% of the value of $pd\pi$ (=0.61 eV) obtained for the Fe-O distances averaged over all $B$ sites (2.059 Å). Similarly the relative difference is 31% for the $Cc$ lattice structure data in Ref. 31. Note that it is the symmetry of the order in the initial state that determines the main features of energy and polarization dependence of the reflection intensities rather than precise choice of individual parameters presented here. The exchange splitting caused by ferrimagnetism $\mu_{\rm B}H_{\rm mol} = 0.08$ eV along the $c_{\rm m}$ axis is also applied. $\Gamma = 0.2$ eV (0.3 eV) at the $L_3$ ($L_2$) edges is assumed in Eq. (13) and a Gaussian broadening with a width of 0.15 eV (HWHM) is applied for the intensity curves of the reflections.

### 2. *Possibility of ROO-CO*

We first discuss the $(00\frac{1}{2})_c$ reflection intensities below $T_{\rm V}$ employing the ROO-CO state proposed by the LDA + $U$ band structure theory,[28,29] which is obtained with the pseudo-$Pmca$ lattice structure,[10] as the initial state of the cluster model calculations. The same atomic positions used in the band structure calculations are assumed in our calculations. The resultant $t_{2g}$ orbital occupations on the "$Fe^{2+}$" sites are the same as the ROO-CO state found in the band structure calculations [see Fig. 1(a)]. The wave functions of the $3d$ orbitals are compared with those of LDA + $U$ results presented in Table I in Ref. 30 and the value of the trigonal field parameter $D_{\rm trg} = 0.05$ eV is adopted to have the most accurate fit. The values of $w^{(2+)}$ are chosen so as to reproduce the occupation number of the minority-spin $t_{2g}$ orbital of the table: $w^{(2+)} = 0.8\,(w^{(3+)} = 0.2)$ for the "$Fe^{2+}$" sites ($B1a,b$ and $B4$ sites) and $w^{(2+)} = 0.2\,(w^{(3+)} = 0.8)$ for the "$Fe^{3+}$" sites ($B2a,b$ and $B3$ sites). The difference in the $t_{2g}$ orbital occupation between the "$Fe^{2+}$" and "$Fe^{3+}$" sites is $\delta n_{t2g} = 0.56$ on average. Here, the $3d$ spin-orbit interaction is not included in the initial state, since this induces large orbital moments $\sim 0.5\,\mu_{\rm B}$ at the "$Fe^{2+}$" sites, which are artifacts of the independent cluster approximation and contradict the result of band structure calculations.

Figure 7 shows calculated energy and polarization dependence of the $(00\frac{1}{2})_c$ reflection intensities for various azimuth angles with ROO-CO in the initial state. The solid (dashed) lines denote the intensities with $\sigma$-polarization ($\pi$-polarization) light. The azimuth angle dependence of their integrated intensities are also drawn on the right. The spectra for the single-domain crystal with the $(0,0,1)_{\rm m}$ magnetization direction are shown in (b), and those obtained assuming Eq. (7) for the $Fe_3O_4$ layer on the stepped MgO substrate in (a). It is clear from Fig. 7(a) that the shapes of the integrated-intensity curves are in between those in Figs. 6(a) and 6(b), and the symmetry of the ROO-CO state is thus pseudo-$P\underline{mc}a$. This is not surprising, since the orbital alignment of the ROO-CO state, as done in these calculations, is induced merely by the distortion of the oxygen octahedrons due to the pseudo-$Pmca$ lattice deformation. The shapes of the spectra are remarkably different from those of the experiments and the polarization dependence at 0° has the wrong sign. Particularly, the intensities of peaks A and B are extremely large compared

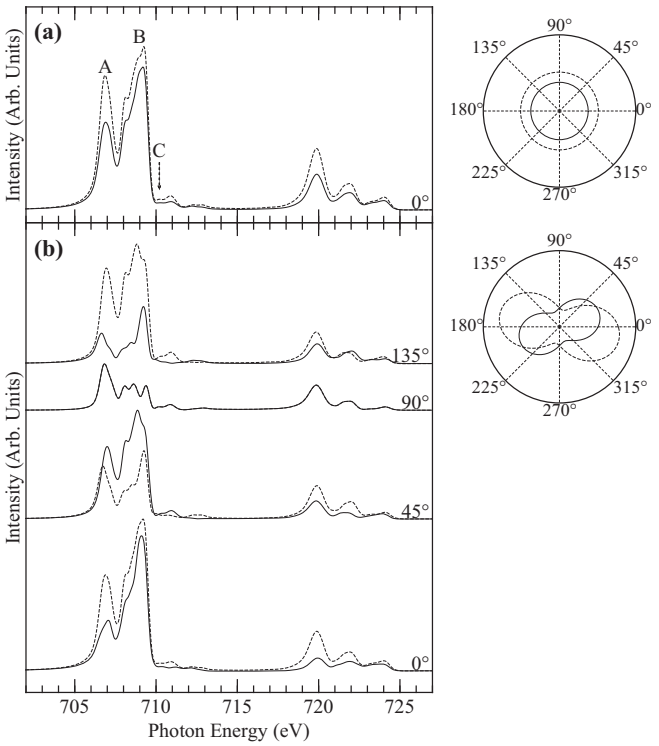


FIG. 7. Theoretical energy and polarization dependence of the $(00\frac{1}{2})_c$ reflection intensities for various azimuth angles with ROO-CO (Ref. 28 and 29) in the initial state obtained with the pseudo-$Pmca$ lattice structure (Ref. 10). The solid and dashed lines denote the intensities with the $\sigma$- and $\pi$-polarization light, respectively. Those for the $Fe_3O_4$ layer on the stepped MgO substrate (a) and for the single domain (b) are depicted. The azimuth angle dependence of integrated intensities are also shown on the right.

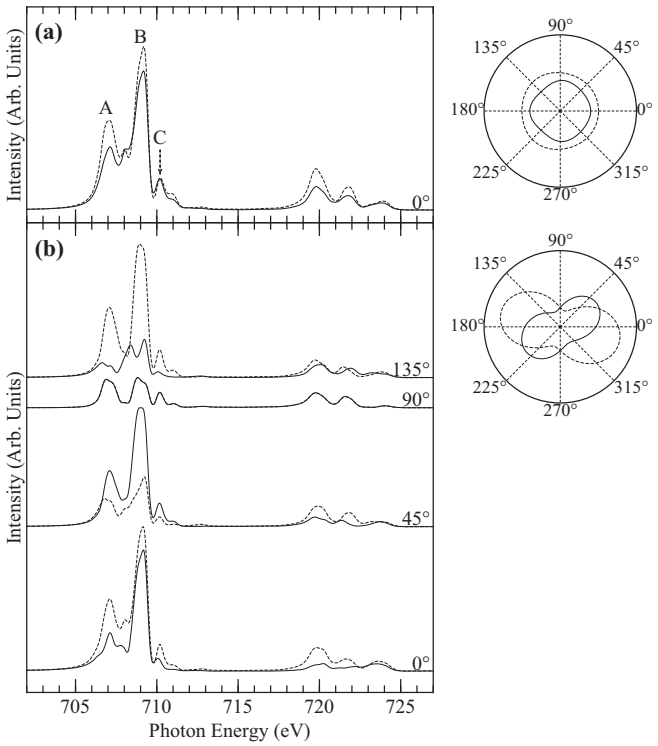


FIG. 8. The same as Fig. 7 but with ROO-CO in the initial state obtained assuming the $Cc$ lattice structure optimized with the GGA + $U$ method (Ref. 31).

with the experiments. The small peak C mainly originates from the "$Fe^{3+}$" states.

The $B1$ and $B4$ sites mainly contribute to the reflection intensities for this ROO-CO. Because of the lack of terms with the diagonal elements of scattering matrix $F_{xx}$ and $F_{yy}$ in Eq. (3), the scattering does not arise if the occupied orbitals of minority spin at the $B4$ sites are pure $XY$ $(x^2 - y^2)$ orbitals. Instead, on-site hybridization of $\frac{1}{\sqrt{2}}(|ZX\rangle - |YZ\rangle)$ $(= |yz\rangle)$ with $|XY\rangle$ for the wave function of the occupied orbital is responsible for the scattering corresponding to the term with $F_{yz}$. Similarly, the scattering at $B1$ sites does not occur with pure $YZ/ZX$ orbital alignment and only the presence of $|XY\rangle$ component in these occupied orbitals is the cause of the scattering.

Having found that the symmetry of the ROO-CO state obtained with the pseudo-$Pmca$ lattice is too high to explain the experimental $(00\frac{1}{2})_c$ intensities, we next examine the ROO-CO state in the $Cc$ symmetry predicted with the GGA + $U$ approach.[31] The atomic positions in the $\sqrt{2}a_c \times \sqrt{2}a_c \times 2a_c$ supercell with the $Cc$ symmetry optimized with the GGA + $U$ method in Ref. 31 are adopted in the calculations. Again, with this $Cc$ lattice structure, essentially the same alignment of the occupied $t_{2g}$ orbitals on the "$Fe^{2+}$" sites to the GGA + $U$ calculations are obtained in the initial state. The parameters $D_{\rm trg} = 0.05$ eV, $w^{(2+)} = 0.8$ for the "$Fe^{2+}$" sites and $w^{(2+)} = 0.2$ for the "$Fe^{3+}$" sites are chosen. Compared to the ROO-CO state with the pseudo-$Pmca$ symmetry, one of the $Fe^{2+}$ ions on four crystallographically unique $B$ sites corresponding to $B4$ sites in $Pmca$ is replaced by a $Fe^{3+}$ ion and one of the $Fe^{3+}$ ions on four unique $B$ sites corresponding to $B2$ sites in $Pmca$ is replaced with a $Fe^{2+}$ ion having a dominantly occupied $XY$ orbital.

In Fig. 8, theoretical energy and polarization dependence of the $(00\frac{1}{2})_c$ reflection intensities for various azimuth angles with ROO-CO obtained assuming the $Cc$ lattice structure are presented. Note that since the crystal is polar with $Cc$, the intensities of the single-domain crystal with the $(001)_{\rm m}$ magnetization direction in Fig. 8(b) and those with the same magnetization direction and the crystal rotated around the $b_{\rm m}$ axis by 180° (not shown) are substantially different. Two directions of magnetization $(0,0, \pm 1)_{\rm m}$ and twinning due to four orientations of the crystal (±45° rotation of the crystal around the $c_{\rm m}$ axis and two polar directions) are considered for the intensities of the $Fe_3O_4$ layer on the stepped MgO substrate in Fig. 8(a). The shapes of the spectra are rather similar to those obtained with the pseudo-$Pmca$ lattice structure in Fig. 7 except for the reduction of the intensity of peak A and the increase of the intensity of peak C. Because of the symmetry lowering, a small azimuth angle dependence in the polar plots of integrated intensities in Fig. 8(a) can be seen. However, this effect of the monoclinic distortion is minor and cannot account for the conspicuous angular dependence of the intensity found in the experiments. This is because the charge and orbital pattern on individual atomic layers parallel to the $a_{\rm m}$-$b_{\rm m}$ plane still has a pseudo-$\sigma_a$ mirror symmetry despite no distinct position of the $\sigma_a$ mirror plane shared by all the

layers, and therefore has no pseudo-orthorhombic symmetry (note that all the phase factors of the $B$ sites are the same within each layer for the $(00\frac{1}{2})_c$ reflection, and thus mutual shifts of $\sigma_a$ mirror planes among layers do not affect the intensities).

### 3. *Possibility of COO*

The COO state proposed in Ref. 32 has a true monoclinic $P2/c$ symmetry [see Fig. 1(b)]. This COO state is stabilized, even if an approximated $Pmca$ lattice structure with no monoclinic distortion ($\beta = 90^\circ$) is assumed. This spontaneous symmetry breaking toward $P2/c$ within the $3d$ electronic state is prominent as seen in Table I, where large differences in the orbital moments as well as the orbital occupations between the $B1a$ and $B1b$ sites and also the $B2a$ and $B2b$ sites are found (those are equivalent sites in $Pmca$); the $\sigma_a$ mirror symmetry is removed at the $B3$ and $B4$ sites. Note that the $t_{2g}$ orbitals with the largest occupation numbers at the $B1a$ and $B1b$ sites are the $YZ$ and $ZX$ orbitals, respectively, and these orbital occupations are consistent with the Jahn-Teller-like distortions found in the experiments.[10] Unlike the ROO-CO states discussed before, the large orbital moments ($\sim 0.46\,\mu_B$ on average) are induced in the $B$ sites. The charge disproportion among the $B$ sites is small and at most $\delta n_{t2g} \sim 0.2$ in this COO state.

To calculate the RXD intensities for the COO state, the occupied minority-spin $t_{2g}$ orbital in each of the $FeO_6$ clusters in the initial state is required to be the same as on the corresponding $B$ site in the COO state obtained with the spinless three-band Hubbard model in Ref. 32. For this purpose, the $3\times3$ density matrix $\langle c^\dagger_{l\nu} c_{l\mu}\rangle$ of the minority-spin $t_{2g}$ orbitals in each site $l$ obtained from the three-band Hubbard model is diagonalized and the maximally occupied orbital $|\psi_l\rangle$, i.e., the eigenfunction having maximum eigenvalue $n^{(l)}_{\max}$, is extracted. The eigenvalue $n^{(l)}_{\max}$ and coefficients $C^{(l)}_\mu$ of the eigenfunction $|\psi_l\rangle = C^{(l)}_{YZ}|YZ\rangle + C^{(l)}_{ZX}|ZX\rangle + C^{(l)}_{XY}|XY\rangle$ on each site are listed in Table I. Since $n^{(l)}_{\max}$ is found to be more than 95% of the total occupation number $n^{(l)}_{t2g}$ of the minority-spin $t_{2g}$ orbital of the site, in the calculations it is assumed that the probability of the $Fe^{2+}$ state occurring at site $l$ is $w^{(2+)}_l = n^{(l)}_{t2g}$ and that the minority-spin $\psi_l$ orbital is occupied in each $Fe^{2+}$ state. To produce such a ground state, the energy of orbital $\psi_l$ is lowered by $D_{\rm cpx} = 0.15$ eV relative to the other two $t_{2g}$ states as

$$H^{(l)}_{\rm cpx} = D_{\rm cpx}\left(\tfrac{1}{3}P_{t2g} - |\psi_l\rangle\langle\psi_l|\right) \qquad (15)$$

and an octahedral crystal field with $10Dq = 0.7$ eV is assumed instead of using Eq. (12) in the initial state. For the final state, Eq. (12) with $D_{\rm trg} = 0$ eV is adopted. The atomic positions of the pseudo-$Pmca$ lattice in Ref. 10 are used in the calculations. The $3d$ spin-orbit interaction in the initial state is included and this causes small canting of the spin moment from the $c$ axis in each $B$ site due to the noncollinear alignment of the orbital moments. The sizes of the $x$ or $y$ components of the spin moments induced by these effects are small and at most $\sim 0.16\,\mu_B$.

Figure 9 shows calculated energy and polarization dependence of the $(00\frac{1}{2})_c$ reflection intensities for various azimuth angles with the COO with $P2/c$ in the initial state. The

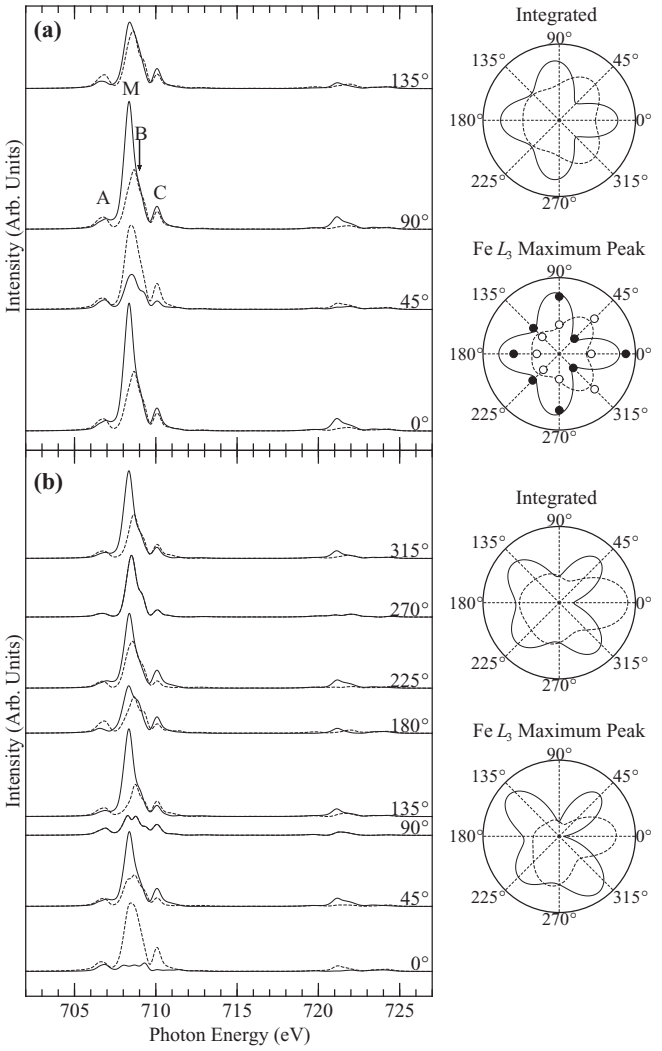


FIG. 9. Theoretical energy and polarization dependence of the $(00\frac{1}{2})_c$ reflection intensities for various azimuth angles with the COO state with $P2/c$ symmetry (Ref. 32) in the initial state. The solid and dashed lines denote the intensities with the $\sigma$- and $\pi$-polarization light, respectively. Those for the $Fe_3O_4$ layer on the stepped MgO substrate (a) and for the single domain (b) are drawn. On the right, polar plots of Fe $L_3$ maximum peak (at 708.3 eV) and integrated intensities are shown as a function of azimuth angle; for comparison, experimental integrated intensity of $L$ scan at Fe $L_3$ maximum of the $Fe_3O_4$ layer on the stepped MgO substrate with $\sigma$ ($\pi$) polarized light in Ref. 47 are depicted together as closed (open) circles.

large azimuth angle dependence of the Fe $L_3$ maximum peak and integrated intensities on the right-hand side in Fig. 9(a) reflect the monoclinic nature of the COO state [see Fig. 6(c)]. The polar plot of Fe $L_3$ maximum peak intensity of the $\sigma$-polarization light has four maxima at 0°, 90°, 180°, and 270° and the clear dips at 45° and 315°, where intensities of the $\sigma$- and $\pi$-polarization light are reversed. Together with the shape of the $\pi$-polarization curve, these features of the $\sigma$-polarization curve are consistent with experimental intensities of the $Fe_3O_4$ layer on the stepped MgO substrate (shown as circles in the same figure). A single intensive peak at $\sim$708.3 eV accompanied by the weak shoulder and satellite structures observed in the experimental spectra at the $L_3$ edge

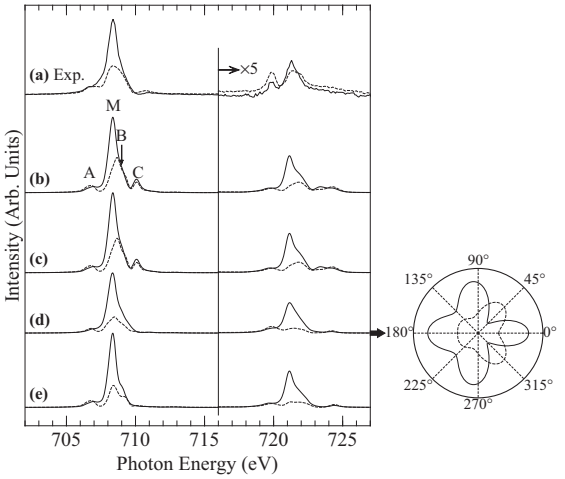


FIG. 10. Experimental (a) and theoretical (b)–(e) energy and polarization dependence of the $(00\frac{1}{2})_c$ reflection intensities with $\phi = 0^\circ$. The intensities of spectra at $L_2$ edge are enhanced by a factor 5 relative to those at $L_3$ edge. All the effects are considered in (b). In (c), the monoclinic displacements of the $B$ sites are omitted but the $3d$–O $2p$ hybridization and crystal field are kept the same as for (b). The spectra calculated without the monoclinic displacements of the oxygen and $B$ sites are shown in (d); (e) is the same as (b) but the contribution of the $Fe^{3+}$ states is neglected. For the experimental spectra, backgrounds are subtracted using the same procedure as in Ref. 45.

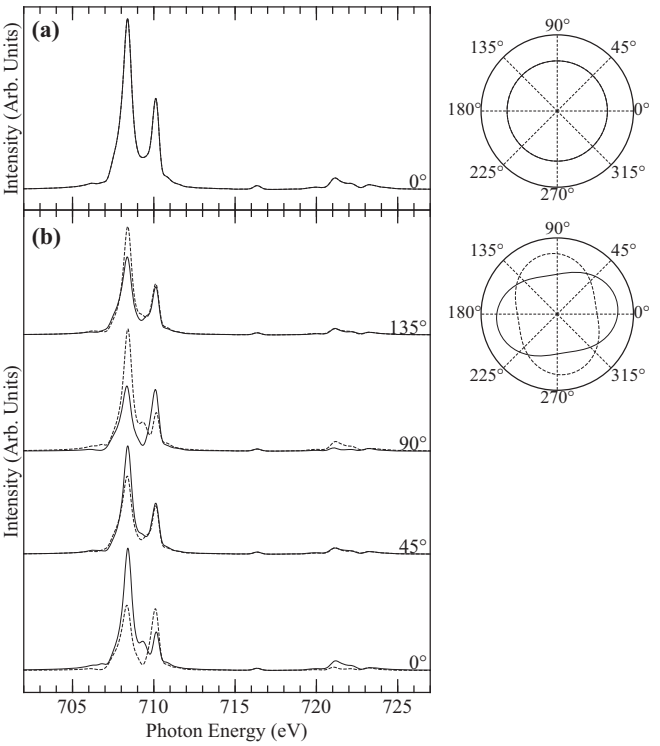


FIG. 11. The same as Fig. 9 but for the $(001)_c$ reflection. On the right, polar plots of integrated intensities are shown as a function of azimuth angle.

are also well reproduced in the theoretical spectra [the main peak M and structures A, B, and C at the $L_3$ edge in Fig. 9(a)].

#### 4. *Orbital order versus lattice distortion*

Having found that the experimental $(00\frac{1}{2})_c$ reflection intensities can be explained well with the COO state, we now discuss the cause of the reflection intensities more in detail. In Fig. 10, the experimental (a) and theoretical (b)–(e) energy and polarization dependence of the $(00\frac{1}{2})_c$ reflection intensities with $\phi = 0^\circ$ are compared. All the effects are considered in the spectra in (b), which are identical to those with $\phi = 0^\circ$ in Fig. 9(a), while some effects are omitted in the other theoretical spectra for comparison. In (c), the monoclinic displacements of the $B$ sites are neglected but the $3d$–O $2p$ hybridization and crystal field are kept the same as for (b). The spectra calculated without monoclinic displacements of both the oxygen and $B$ sites are shown in (d); (e) is the same as (b) but the contribution of the $Fe^{3+}$ states is neglected ($w_l^{(3+)} = 0$ are assumed, while $w_l^{(2+)}$ are not changed).

The monoclinic distortion affects the intensity in Eq. (14) in two ways: the shifts of the phases $\exp(i\boldsymbol{q}\cdot\boldsymbol{R}_l)$ caused by the atomic displacements of the $B$ sites and variations in the scattering factors $f_l$. Since only slight difference can be seen by the removal of the former effects as in Fig. 10(c), variations in $f_l$'s mainly contribute to the spectra. Such changes in $f_l$ can be caused by modification of the intermediate-state $3d$ levels owing to the displacement of surrounding oxygen atoms, and ordering in the $3d$ state in the initial state. If all the intermediate-state effects are removed as in Fig. 10(d), substantial change in their shapes can be found: the intensity ratio of the reflections with the $\sigma$- and $\pi$-polarized light is changed and peak C is diminished. On the other hand, the strong azimuth angle dependence of the integrated intensities, which is the signature of the monoclinic symmetry, is retained (the polar plots in Fig. 10). These results show clearly that although the intermediate-state effects cannot be neglected, the azimuth angle dependence mainly originates from the symmetry of the $3d$ electronic state in the initial state, i.e., the orbital order.

From Fig. 10(e), it is clear that the majority of the $(00\frac{1}{2})_c$ reflection intensities is due to the $Fe^{2+}$ states and only peak C with its weak intensity is dominantly caused by the $Fe^{3+}$ states. This is because the multiplet of the ground state within the $O_h$ symmetry of the $Fe^{2+}$ states is ${}^5T_2$ and $T_2 \times T_2 = A_1 + E + T_1 + T_2$ contains the $T_2$ and $E$ bases corresponding to the scattering matrices $F_{yz}$, $F_{zx}$, and $F_{xy}$ appearing in Eq. (4), whereas that for the $Fe^{3+}$ states is ${}^6A_1$ and $A_1 \times A_1 = A_1$ does not include $T_2$ nor $E$. The contribution from the $Fe^{3+}$ states is, therefore, due to the intermediate-state effects. This is also evident in Fig. 10(d), where peak C is diminished.

The intensity integrated over the $L_2$ edge region relative to that of $L_3$ edge of the experimental spectra is extremely weak. The ratio of the integrated intensities between these two edges is quantitatively in accordance with theoretical spectra obtained with the COO state in the initial state. In contrast, the ratio is much larger in the spectra obtained with the ROO-CO states in the initial state (see Figs. 7 and 8).

#### 5. $(001)_c$ *reflection and charge disproportionation*

In Fig. 11, theoretical energy and polarization dependence of the $(001)_c$ reflection intensities are depicted for various

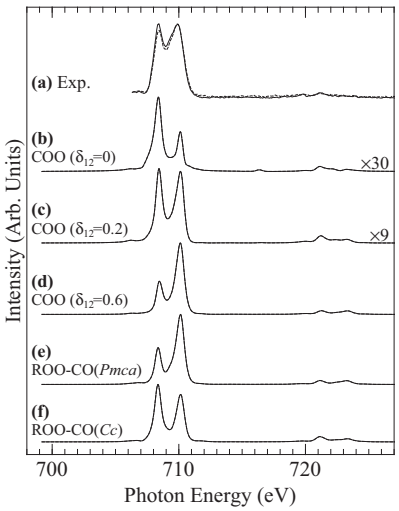


FIG. 12. Experimental (a) and theoretical (b)–(f) energy dependence of the $(001)_c$ reflection intensities with $\phi = 0°$. To show the effects of charge disproportion, in (b)–(d) the values of $n_{t2g}^{(l)}$ $(= w_l^{(2+)})$ are increased by $\delta_{12}/2$ for the $B1$ sites and decreased by $\delta_{12}/2$ for the $B2$ sites from the values of the COO state in Table I: in (b) $\delta_{12} = 0$ [the same to Fig. 11(a)], in (c) $\delta_{12} = 0.2$, and in (d) $\delta_{12} = 0.6$. Those for the ROO-CO with $P\underline{mc}a$ (e) and $C\underline{c}$ (f) symmetries are also depicted. Here, $\theta = \pi/2$ is assumed in the theoretical intensities and thus those with the $\sigma$- and $\pi$-polarization light are identical. For the experimental spectra, backgrounds are subtracted using the same procedure as in Ref. 45.

azimuth angles with the COO with $P2/\underline{c}$ symmetry in the initial state. The integrated intensities are about 10 times larger than those of the $(00\frac{1}{2})_c$ reflection. Unlike the $(00\frac{1}{2})_c$ reflection, no indication for azimuthal dependence was found for the experimental $(001)_c$ reflection, which is consistent with the theoretical results in Fig. 11(a). The main features of the experimental spectra in Fig. 12(a), e.g., the double-peak structure and relative peak positions at the $L_3$ edge, and no polarization dependence, are well captured by our calculation except for smaller intensity of the high-energy peak at the $L_3$ edge as compared to experimental one. The lower (higher) energy peak at the $L_3$ edge mainly arises from the $Fe^{2+}$ ($Fe^{3+}$) states. For the $(001)_c$ reflection, the optical process where an electron in the Fe $2p$ core is excited to and returned from one of the totally empty minority-spin $3d$ levels without any orbital scattering is allowed by the diagonal components of the scattering matrices in Eq. (9) and is the dominant process for the $Fe^{3+}$ states. Since this process is not involved with the orbital order, the intensities due to the $Fe^{3+}$ states are proportional to the square of the difference between averaged $w_l^{(2+)}$ of the $B1$ sites and that of the $B2$ sites (the contributions of the $B3$ and $B4$ sites are small as discussed in Sec. IV A).

To see how charge disproportionation affects the reflection intensities, in Fig. 12, those for COOs obtained with the values of $n_{t2g}^{(l)}$ $(= w_l^{(2+)})$ increased by $\delta_{12}/2$ for the $B1$ sites and decreased by $\delta_{12}/2$ for the $B2$ sites from the values in Table I are presented in (b)–(d) together with the experimental intensity (a) and that for the ROO-COs with $P\underline{mc}a$ (e) and $C\underline{c}$ (f) symmetries. The averaged $n_{t2g}$ of the $B1$ sites and that of the $B2$ sites in the COO state are nearly the same, and the weak intensity in the high-energy peak in (b) is caused by not the charge order but the intermediate-state effects. As seen in the figure, the intensities of the high-energy peak are approximately proportional to $\delta_{12}^2$ apart from this small contribution of the intermediate-state effects. The experimental intensity curve is reproduced well with $\delta_{12} = 0.2$. On the other hand, the intensity curve for the COO with a large $t_{2g}$ charge disproportion $\delta_{12} = 0.6$ is inconsistent with the experimental curve.

The intensity ratio of the double peak for the ROO-CO with $P\underline{mc}a$ symmetry in Fig. 12(e) largely deviates from that of the experiments. To reproduce the experimental peak ratio, the $t_{2g}$ charge disproportion between the "$Fe^{2+}$" and "$Fe^{3+}$" sites needs to be reduced to $\delta n_{t2g} = 0.18$, which is much smaller than the value of the LDA + $U$ band structure calculations $\delta n_{t2g} = 0.56$ adopted in Fig. 12(e) (see Table I in Ref. 30). On the other hand, reasonably good agreement with experiments can be found for the intensity curve of the ROO-CO with $C\underline{c}$ symmetry in Fig. 12(f). In this case, only a slight increase $\sim$0.1 of the value of $\delta n_{t2g}$ is enough to obtain the same peak ratio as seen in the experiments. The weaker intensity of the high-energy peak relative to that of the ROO-CO with $P\underline{mc}a$ symmetry is mainly because 1/4 of the $B$ sites corresponding to the $B2$ sites in $Pmca$ are "$Fe^{2+}$" sites instead of "$Fe^{3+}$" sites in this order; i.e., $\delta_{12} = 3\delta n_{t2g}/4$.

## V. DISCUSSION AND REMARKS

So far we have discussed the $(00\frac{1}{2})_c$ reflection intensities at the Fe $L_{2,3}$ resonance from $Fe_3O_4$ below $T_V$. We have found that the azimuth dependence of RXD is more sensitive to the electronic state than that of the lattice and in fact revealed that the electronic state below $T_V$ has a large monoclinic deformation with the value of $\mathrm{Re}[F_{xy}]/\mathrm{Re}[F_{yz}] \sim 2$. This distinct feature of RXD at the transition-metal $L_{2,3}$ edges stems from its sensitivity to the initial-state wave function, unlike what has been claimed by Wilkins *et al.* in Ref. 42. This can be contrasted with RXD at the transition-metal $K$ edge, where the intermediate-state effects, i.e., changes in excitation levels due to the shifts of surrounding atom positions relative to the excited site, are dominant, and therefore information of the $3d$ state cannot be easily separated from that of the lattice.[34,35]

The fact that the order which occurs below $T_V$ has a large monoclinic deformation extremely restricts plausible theories on the Verwey transition, since the majority of them so far proposed assume charge or orbital orders with the orthorhombic symmetry or at most those with small monoclinic deformations. In addition to the azimuth and polarization dependence of the intensity, examination of the photon energy dependence, i.e., the multiplet structures, permits us to impose further restriction on possible models for orbital, charge, and magnetic order in the initial state. Indeed, while COO remains as a possible order in the low-temperature phase of magnetite, two ROO-CO models predicted by band structure calculations are found to be ruled out by the analysis with the configuration-interaction cluster model and comparison with experimental results.

These aspects of RXD at the transition-metal $L_{2,3}$ edges have been already pointed out in a pioneering work of

Castleton and Alterelli on manganite[36] and our previous work on $La_{2-x}Sr_xNiO_4$.[41] We would like to stress that RXD at the transition-metal $L_{2,3}$ edges with azimuth and polarization analysis is particularly sensitive to the $3d$ electronic state, and therefore a technique complementary to other x-ray or neutron diffraction methods.

The main difficulty to know the true ordered state below $T_V$ in $Fe_3O_4$ has been the rather small distortion of the lattice and lack of a precise knowledge of the lattice structure, from which charge or orbital order in the crystal usually can be deduced. With the aid of RXD, we have directly detected the presence of the orbital order in the $t_{2g}$ orbitals of $B$ sites below $T_V$ without knowing detailed information of the lattice structure and revealed that the order has a large monoclinic deformation, which is consistent with the COO theory.

In their very recent high-energy x-ray diffraction study with almost single-domain $Fe_3O_4$ nanograins, Senn *et al*. reported detailed atomic positions of the full $Cc$ superstructure.[13] With this structure essentially the same charge and orbital order pattern predicted in Ref. 31 except for the difference in the occupied $t_{2g}$ orbital at $B8$ site has been obtained by DFT+$U$ calculations.[60] Nearly the same COO state obtained with the pseudo-$Pmca$ structure is also stabilized with the $Cc$ structure by Senn *et al*. using the three-band model in Ref. 32. Despite the apparent large differences between the COO and ROO-CO states, the maximally occupied orbitals of every $Fe^{2+}$ site coincide with each other. Therefore the stabilization of the COO state with the $Cc$ structure can be explained by the same mechanism as the trimeron proposed by Senn *et al*., where the lobes of the dominantly occupied orbital in each site extend toward the directions of unoccupied orbitals of nearby $B$ sites, lowering the kinetic energy.

Although two of the ROO-CO states discussed in this paper are not compatible with the RXD results, there still remain possibilities of ROO-CO states with larger monoclinic deformations below $T_V$. The fundamental difference between ROO-CO and COO is whether large orbital moments $\sim 0.5\mu_B$ are present on $B$ sites or not. The size of the ferromagnetic component of the orbital moments on $B$ sites in magnetite has been debated and different values have been inferred from the measurements of the Fe $L_{2,3}$ x-ray absorption spectra with circularly polarized light.[61–67] However, the presence of the ferromagnetic component of the orbital moments on the $B$ sites alone does not constitute strong evidence of the existence of the COO state, since the component can be merely induced by the ordered spins through the spin-orbit interaction as in many other magnetic compounds. It is, therefore, essential to detect the antiferromagnetic, i.e., noncollinear, component of the orbital moments more directly by measuring the size of the term $\mathrm{Im}[F_{zx}]$ of the RXD, which appears only with magnetic space group, using circularly polarized light with a magnetic applied field on the sample. Such RXD experiments would enable one to further characterize the order below $T_V$ and would be interesting for future research.

## VI. CONCLUSIONS

A thin layer of $Fe_3O_4$ partially detwinned by growth on the stepped MgO(001) substrate is studied by resonant soft x-ray diffraction at the Fe $L_{2,3}$ edges to investigate the charge and orbital order below $T_V$. The azimuth angle, incident photon polarization, and energy dependence of the $(00\frac{1}{2})_c$ and $(001)_c$ reflection intensities were measured, and analyzed with the configuration-interaction $FeO_6$ cluster model. In particular, the azimuth angle dependence of the intensities is found to reflect strongly the space-group symmetry of the $3d$ state in the initial state rather than that of the lattice. The analysis of the $(00\frac{1}{2})_c$ reflection intensities shows that the orbital order in the $t_{2g}$ orbitals of $B$ sites below $T_V$ has a large monoclinic deformation with the value of $\mathrm{Re}[F_{xy}]/\mathrm{Re}[F_{yz}] \sim 2$. This finding extremely limits possible theories on the Verwey transition, since the majority of them so far proposed do not assume charge or orbital orders with such a large monoclinic deformation. Furthermore, the incident photon polarization and energy dependence of the $(00\frac{1}{2})_c$ reflection intensities cannot be explained by the real-number orbital and charge orders predicted by the LDA + $U$ and GGA + $U$ band structure theories in Refs. 28–31 but by the complex-number orbital order in Ref. 32 with a large monoclinic deformation. Charge disproportion among the $t_{2g}$ orbitals of the $B$ sites at least $\delta n_{t2g} \sim 0.2$ is inferred from the analysis of the $(001)_c$ reflection.

## ACKNOWLEDGMENTS

We thank Lucie Hamdan and the mechanical workshop of the II. Physikalische Institut for their skillful technical assistance. This work was supported by the Deutsche Forschungsgemeinschaft through SFB 608 and by the BMBF through Contracts No. 05KS7PK1, No. 05K10PK2, and No. 05ES3XBA/5.

## APPENDIX: BASIS SET REDUCTION

Here, we will briefly explain a method to find an optimal and reduced basis set out of the full 18 (=3×6) bases of the O $2p$ orbital of a slightly distorted $MO_6$ octahedral cluster having a $3d$ transition metal ion $M$ in the center. The hopping integrals between the $3d$ and O $2p$ orbitals on six neighboring oxygen are calculated using the atomic position data. For the Slater-Koster parameters $pd\sigma$ and $pd\pi$, $M$-O bond length $R$ dependence $pdm \propto 1/R^{7/2}$ is assumed after Harrison.[58] A mathematical theorem ensures that the 5×18 hopping matrix $V^{(l)}_{m,n} = \langle 3d\, m|V|2p\, n\rangle$ can be written in a form with a certain choice of $5 \times 5$ $U$ and $18 \times 18$ $W$ unitary matrices as

$$V^{(l)} = U \begin{pmatrix} \lambda_1 & 0 & \cdots & 0 & 0 & 0 & \cdots & 0 \\ 0 & \lambda_2 & \ddots & \vdots & 0 & 0 & \cdots & 0 \\ \vdots & \ddots & \ddots & 0 & \vdots & \vdots & \cdots & \vdots \\ 0 & \cdots & 0 & \lambda_5 & 0 & 0 & \cdots & 0 \end{pmatrix} W. \quad \text{(A1)}$$

From this, one finds that with the transformation of the oxygen $2p$ bases $|w_i\rangle = \sum_n W_{i,n}|2p\, n\rangle$ only five of them $\{|w_i\rangle\}$ ($i = 1, \ldots, 5$) are directly hybridized with the $3d$ orbitals on site $l$. If some of remaining $2p$ bases and any of the $3d$ orbitals have the same point-group symmetry, these $2p$ bases can be indirectly reached from the $3d$ orbitals through the hybridization among the O $2p$ orbitals. However, since the distortion of the cluster from the $O_h$ symmetry is small, this effect can be neglected, and only five molecular orbitals $\{|w_i\rangle\}$ ($i = 1, \ldots, 5$) on the

ligand are retained in the calculations. $U$ and $\lambda_i^2$'s can be easily obtained numerically by diagonalizing a $5 \times 5$ matrix $V^{(l)}V^{(l)\dagger}$. Once $U$ and $\lambda_i^2$'s are known, $W$ can be calculated using the relation

$$W = \mathrm{diag}\left[\lambda_1^{-1}, \lambda_2^{-1}, \ldots, \lambda_5^{-1}\right] U^\dagger V^{(l)}.$$

The hopping matrix between the $3d$ orbitals and redefined molecular orbitals $|\chi_i\rangle \equiv \sum_j U_{i,j}|w_j\rangle$ is described as

$$\tilde{V}^{(l)} = U\,\mathrm{diag}[\lambda_1, \lambda_2, \ldots, \lambda_5]U^\dagger.$$

Note that if the $MO_6$ cluster is a regular octahedron, the bases $\{|\chi_i\rangle\}$ are identical to the $t_{2g}$ and $e_g$ molecular orbitals in the $O_h$ symmetry often used in cluster calculations.


[1] E. J. W. Verwey, Nature (London) **144**, 327 (1939).
[2] For review see F. Walz, J. Phys.: Condens. Matter **14**, R285 (2002); J. García and G. Subías, *ibid.* **16**, R145 (2004).
[3] M. Iizumi and G. Shirane, Solid State Commun. **17**, 433 (1975).
[4] L. V. Gasparov, D. B. Tanner, D. B. Romero, H. Berger, G. Margaritondo, and L. Forró, Phys. Rev. B **62**, 7939 (2000).
[5] Y. Miyamoto and S. Chikazumi, J. Phys. Soc. Jpn. **57**, 2040 (1988).
[6] Y. Miyamoto and M. Shindo, J. Phys. Soc. Jpn. **62**, 1423 (1993).
[7] C. Medrano, M. Schlenker, J. Baruchel, J. Espeso, and Y. Miyamoto, Phys. Rev. B **59**, 1185 (1999).
[8] M. Iizumi, T. F. Koetzle, G. Shirane, S. Chikazumi, M. Matsui, and S. Todo, Acta Crystallogr., Sect. B **38**, 2121 (1982).
[9] J. P. Wright, J. P. Attfield, and P. G. Radaelli, Phys. Rev. Lett. **87**, 266401 (2001).
[10] J. P. Wright, J. P. Attfield, and P. G. Radaelli, Phys. Rev. B **66**, 214422 (2002).
[11] Y. Joly, J. E. Lorenzo, E. Nazarenko, J.-L. Hodeau, D. Mannix, and C. Marin, Phys. Rev. B **78**, 134110 (2008).
[12] J. Blasco, J. García, and G. Subías, Phys. Rev. B **83**, 104105 (2011).
[13] M. S. Senn, J. P. Wright, and J. P. Attfield, Nature (London) **481**, 173 (2011).
[14] E. J. W. Verwey, P. W. Haayman, and F. C. Romeijn, J. Chem. Phys. **15**, 181 (1947).
[15] M. Mizoguchi, J. Phys. Soc. Jpn. **70**, 2333 (2001).
[16] P. Novák, H. Štěpánková, J. Englich, J. Kohout, and V. A. M. Brabers, Phys. Rev. B **61**, 1256 (2000).
[17] J. M. Zuo, J. C. H. Spence, and W. Petuskey, Phys. Rev. B **42**, 8451 (1990).
[18] E. Nazarenko, J. E. Lorenzo, Y. Joly, J. L. Hodeau, D. Mannix, and C. Marin, Phys. Rev. Lett. **97**, 056403 (2006).
[19] J. García, G. Subías, M. G. Proietti, J. Blasco, H. Renevier, J. L. Hodeau, and Y. Joly, Phys. Rev. B **63**, 054110 (2001).
[20] Gloria Subías, Joaquín García, Javier Blasco, M. Grazia Proietti, Hubert Renevier, and M. Concepción Sánchez, Phys. Rev. Lett. **93**, 156408 (2004).
[21] R. J. Goff, J. P. Wright, J. P. Attfield, and P. Radaelli, J. Phys.: Condens. Matter **17**, 7633 (2005).
[22] Shih-Chang Weng, Yen-Ru Lee, Cheng-Gang Chen, Chia-Hung Chu, Yun-Liang Soo, and Shih-Lin Chang, Phys. Rev. Lett. **108**, 146404 (2012).
[23] Joaquin Garcia and Gloria Subias, Phys. Rev. Lett. **109**, 049701 (2012).
[24] J. R. Cullen and E. R. Callen, Phys. Rev. B **7**, 397 (1973).
[25] Y. Yamada, Philos. Mag. B **42**, 377 (1980).
[26] S. K. Mishra, Z. Zhang, and S. Satpathy, J. Appl. Phys. **76**, 6700 (1994).
[27] H. Seo, M. Ogata, and H. Fukuyama, Phys. Rev. B **65**, 085107 (2002).
[28] H.-T. Jeng, G. Y. Guo, and D. J. Huang, Phys. Rev. Lett. **93**, 156403 (2004).
[29] I. Leonov, A. N. Yaresko, V. N. Antonov, M. A. Korotin, and V. I. Anisimov, Phys. Rev. Lett. **93**, 146404 (2004).
[30] I. Leonov, A. N. Yaresko, V. N. Antonov, and V. I. Anisimov, Phys. Rev. B **74**, 165117 (2006).
[31] H.-T. Jeng, G. Y. Guo, and D. J. Huang, Phys. Rev. B **74**, 195115 (2006).
[32] H. Uzu and A. Tanaka, J. Phys. Soc. Jpn. **77**, 074711 (2008).
[33] For example, see S. W. Lovesey, E. Balcar, K. S. Kinght, and J. Fernández Rodríguez, Phys. Rep. **411**, 233 (2005).
[34] I. S. Elfimov, V. I. Anisimov, and G. A. Sawatzky, Phys. Rev. Lett. **82**, 4264 (1999).
[35] M. Benfatto, Y. Joly, and C. R. Natoli, Phys. Rev. Lett. **83**, 636 (1999).
[36] C. W. M. Castleton and M. Altarelli, Phys. Rev. B **62**, 1033 (2000).
[37] S. B. Wilkins, P. D. Spencer, P. D. Hatton, S. P. Collins, M. D. Roper, D. Prabhakaran, and A.T. Boothroyd, Phys. Rev. Lett. **91**, 167205 (2003).
[38] K. J. Thomas, J. P. Hill, S. Grenier, Y.-J. Kim, P. Abbamonte, L. Venema, A. Rusydi, Y. Tomioka, Y. Tokura, D. F. McMorrow, G. Sawatzky, and M. van Veenendaal, Phys. Rev. Lett. **92**, 237204 (2004).
[39] S. S. Dhesi, A. Mirone, C. De Nadaï, P. Ohresser, P. Bencok, N. B. Brookes, P. Reutler, A. Revcolevschi, A. Tagliaferri, O. Toulemonde, and G. van der Laan, Phys. Rev. Lett. **92**, 056403 (2004).
[40] U. Staub, V. Scagnoli, A. M. Mulders, K. Katsumata, Z. Honda, H. Grimmer, M. Horisberger, and J. M. Tonnerre, Phys. Rev. B **71**, 214421 (2005).
[41] C. Schüßler-Langeheine, J. Schlappa, A. Tanaka, Z. Hu, C. F. Chang, E. Schierle, M. Benomar, H. Ott, E. Weschke, G. Kaindl, O. Friedt, G. A. Sawatzky, H.-J. Lin, C. T. Chen, M. Braden, and L. H. Tjeng, Phys. Rev. Lett. **95**, 156402 (2005).
[42] S. B. Wilkins, S. Di Matteo, T. A. W. Beale, Y. Joly, C. Mazzoli, P. D. Hatton, P. Bencok, F. Yakhou, and V. A. M. Brabers, Phys. Rev. B **79**, 201102(R) (2009).
[43] S. R. Bland, B. Detlefs, S. B. Wilkins, T. A. W. Beale, C. Mazzoli, Y. Joly, P. D. Hatton, J. E. Lorenzo, and V. A. M. Brabers, J. Phys.: Condens. Matter **21**, 485601 (2009).
[44] Sergio Di Matteo, J. Phys.: Conf. Ser. **190**, 012008 (2009).
[45] J. Schlappa, C. Schüßler-Langeheine, C. F. Chang, H. Ott, A. Tanaka, Z. Hu, M. W. Haverkort, E. Schierle, E. Weschke, G. Kaindl, and L. H. Tjeng, Phys. Rev. Lett. **100**, 026406 (2008).
[46] C. F. Chang, J. Schlappa, M. Buchholz, A. Tanaka, E. Schierle, D. Schmitz, H. Ott, R. Sutarto, T. Willers, P. Metcalf, L. H. Tjeng, and C. Schüßler-Langeheine, Phys. Rev. B **83**, 073105 (2011).

[47]A. Tanaka, C. F. Chang, M. Buchholz, C. Trabant, E. Schierle, J. Schlappa, D. Schmitz, H. Ott, P. Metcalf, L. H. Tjeng, and C. Schüßler-Langeheine, Phys. Rev. Lett. **108**, 227203 (2012).
[48]D. J. Huang, H.-J. Lin, J. Okamoto, K. S. Chao, H.-T. Jeng, G. Y. Guo, C.-H. Hsu, C.-M. Huang, D. C. Ling, W. B. Wu, C. S. Yang, and C. T. Chen, Phys. Rev. Lett. **96**, 096401 (2006).
[49]F. C. Voogt, T. Fujii, P. J. M. Smulders, L. Niesen, M. A. James, and T. Hibma, Phys. Rev. B **60**, 11193 (1999).
[50]J. A. Moyer, C. A. F. Vaz, E. Negusse, D. A. Arena, and V. E. Henrich, Phys. Rev. B **83**, 035121 (2011).
[51]J. H. Neave, B. A. Joyce, P. J. Dobson, and N. Norton, Appl. Phys. A **31**, 1 (1983).
[52]J. Zhang, J. H. Neave, B. A. Joyce, P. J. Dobson, and P. N. Fawcett, Surf. Sci. **231**, 379 (1990).
[53]B. A. Joyce, J. Cryst. Growth **99**, 9 (1990).
[54]J. Brötz, H. Fuess, T. Haage, and J. Zegenhagen, Phys. Rev. B **57**, 3679 (1998).
[55]J. Brötz and H. Fuess, *Studies of High Temperature Superconductors*, edited by A. Narlikar, Vol. 41 (NOVA Science Publishers, New York, 2002), pp. 129–146.
[56]K. Abe, Y. Miyamoto, and S. Chikazumi, J. Phys. Soc. Jpn. **41**, 1894 (1976).
[57]A. Tanaka and T. Jo, J. Phys. Soc. Jpn. **63**, 2788 (1994).
[58]W. A. Harrison, *Electronic Structure and the Properties of Solids* (Freeman, San Francisco, 1980).
[59]J. Chen, D. J. Huang, A. Tanaka, C. F. Chang, S. C. Chung, W. B. Wu, and C. T. Chen, Phys. Rev. B **69**, 085107 (2004).
[60]M. S. Senn, I. Loa, J. P. Wright, and J. P. Attfield, Phys. Rev. B **85**, 125119 (2012).
[61]E. Goering, Phys. Status Solidi B **248**, 2345 (2011).
[62]J.-S. Kang, G. Kim, H. J. Lee, D. H. Kim, H. S. Kim, J. H. Shim, S. Lee, H. G. Lee, J.-Y. Kim, B. H. Kim, and B. I. Min, Phys. Rev. B **77**, 035121 (2008).
[63]D. J. Huang, C. F. Chang, H.-T. Jeng, G. Y. Guo, H.-J. Lin, W. B. Wu, H. C. Ku, A. Fujimori, Y. Takahashi, and C. T. Chen, Phys. Rev. Lett. **93**, 077204 (2004).
[64]E. Goering, M. Lafkioti, and S. Gold, Phys. Rev. Lett. **96**, 039701 (2006).
[65]E. Goering, S. Gold, M. Lafkioti, and G. Schütz, Europhys. Lett. **73**, 97 (2006).
[66]E. Goering, M. Lafkioti, S. Gold, and G. Schuetz, J. Magn. Magn. Mater. **310**, e249 (2007).
[67]A. Yamasaki, H. Kobori, H. Osawa, T. Nakamura, and A. Sugimura, J. Phys.: Conf. Ser. **150**, 042235 (2009).